Journal of Medicinal Chemistry

pubs.acs.org/jmc

Article

Pyrrolo[2′,3′:3,4]cyclohepta[1,2-*d*][1,2]oxazoles, a New Class of Antimitotic Agents Active against Multiple Malignant Cell Types

Virginia Spanò,◇ Roberta Rocca,◇ Marilia Barreca,◇ Daniele Giallombardo, Alessandra Montalbano,* Anna Carbone, Maria Valeria Raimondi, Eugenio Gaudio, Roberta Bortolozzi, Ruoli Bai, Pierfrancesco Tassone, Stefano Alcaro, Ernest Hamel, Giampietro Viola, Francesco Bertoni, and Paola Barraja

Cite This: *J. Med. Chem.* 2020, 63, 12023−12042

Read Online

ACCESS | Metrics & More | Article Recommendations | Supporting Information

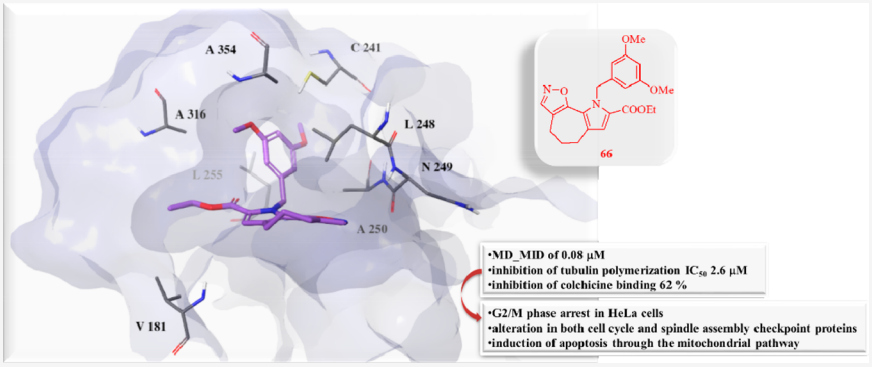

ABSTRACT: A new class of pyrrolo[2′,3′:3,4]cyclohepta[1,2-*d*][1,2]oxazoles was synthesized for the treatment of hyperproliferative pathologies, including neoplasms. The new compounds were screened in the 60 human cancer cell lines of the NCI drug screen and showed potent activity with GI_{50} values reaching the nanomolar level, with mean graph midpoints of 0.08−0.41 μM. All compounds were further tested on six lymphoma cell lines, and eight showed potent growth inhibitory effects with IC_{50} values lower than 500 nM. Mechanism of action studies showed the ability of the new [1,2]oxazoles to arrest cells in the G2/M phase in a concentration dependent manner and to induce apoptosis through the mitochondrial pathway. The most active compounds inhibited tubulin polymerization, with IC_{50} values of 1.9−8.2 μM, and appeared to bind to the colchicine site. The G2/M arrest was accompanied by apoptosis, mitochondrial depolarization, generation of reactive oxygen species, and PARP cleavage.

INTRODUCTION

Microtubules are intracellular polymers involved in the regulation of a large number of cellular processes, including proliferation, division, determination and maintenance of cellular shape, motility, and intracellular transport.[1] They are highly dynamic structures composed of multiple heterodimers of α- and β-tubulin, and they undergo alternating polymerization and depolymerization phases.[2] Disrupting this dynamic equilibrium interferes with cell division and leads to cell death. Tubulin and its associated structures represent an attractive target in the treatment of cancer.[3] Over the past 40 years, a large number of natural and synthetic compounds interfering with microtubule dynamics through interactions with multiple binding sites on tubulin have been described.[4] On the basis of their effects on microtubule dynamics, they can be classified as either microtubule-stabilizing agents or microtubule-destabilizing agents.[5] Among natural derivatives, taxanes, e.g., paclitaxel and docetaxel, belong to the first group of compounds, while vinca alkaloids, e.g., vinflunine, vinorelbine, vincristine, and colchicine, belong to the second group.[6] Despite the large number of new promising drug candidates, no molecules binding at the colchicine site have been approved thus far for the treatment of cancer, leaving the drug discovery process still open.[7,8] Since its discovery, combretastatin A-4 (CA-4) is still considered a promising lead compound binding at the colchicine site (Chart 1).[9] It inhibits tubulin polymerization with low IC_{50} values,[10] and it presents a potent activity against multiple cancer cell lines, including cells bearing a multidrug resistance (MDR) phenotype.[11] In addition to its antimitotic activity, CA-4 can interfere with tumor vasculature, essential for solid tumor survival, leading to necrosis of tumor tissues.[12]

Received: July 29, 2020
Published: September 28, 2020

Chart 1. Structures of Tubulin Polymerization Inhibitors

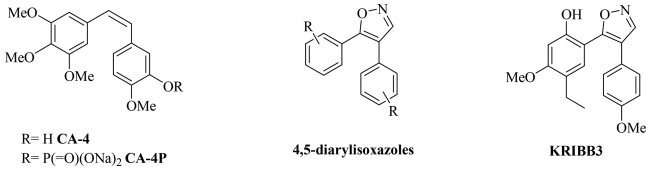

Nevertheless, due to its poor water solubility, low bioavailability, and rapid clearance, CA-4 exhibits poor activity *in vivo*, thus leading to the synthesis of different water-soluble prodrugs including CA-4 phosphate disodium (CA-4P) (Chart 1). In different preclinical models, CA-4P reduces blood flow and causes tumor cell death due to changes in the morphology of immature endothelial cells resulting from interference with tubulin polymerization.[13] As the *cis*-configuration of the olefinic double bond is essential for the antiproliferative activity of CA-4, this bond has been fixed through its incorporation into five- or six-membered heterocycle rings.[12,14,15] The 4,5-diarylisoxazoles showed potent antitumor activity in inducing cell cycle arrest at the G2/M phase of the cell cycle and potent antitubulin activity (Chart 1).[16,17] KRIBB3 (Chart 1), belonging to the same class, displayed antiproliferative activity through inhibition of microtubule polymerization and spindle assembly checkpoint activation. In *in vivo* models, KRIBB3 caused a 50−70% reduction of tumor growth at a dose of 50−100 mg/kg.[18,19]

Isoxazoles or [1,2]oxazoles represent the core structure of many drug candidates. Due to its ability to form multiple noncovalent interactions with a wide number of proteins, this moiety confers different biological activities, such as antitumor, antinflammatory, antidepressant, antiviral, antibacterial, and antitubercolosis activities.[20−27] A series of 5-(1*H*-indol-5-yl)-3-phenylisoxazoles have anticancer activity.[28] Several small molecules containing the indole moiety have also been described as potent tubulin polymerization inhibitors.[29−32]

Our research group has devoted much effort to the synthesis and evaluation of the biological properties of fused tricyclic systems incorporating the pyrrole ring.[33−41] Since the [1,2]oxazole system is found as a pharmacophore moiety of several compounds with promising antitumor properties, we started a program investigating different classes of pyrazole- and pyrrole-fused systems of types **1**, **2**, and **4**, incorporating the [1,2]oxazole unit (Figure 1).[42−45] In particular, from the class of [1,2]oxazole of type **2**, ethyl 8-(3,5-dimethoxybenzyl)-5,8-dihydro-4*H*-[1,2]oxazolo[4,5-*g*]indole-7-carboxylate **3** emerged for its *in vitro* nanomolar growth inhibitory effects across the National Cancer Institute (NCI) cancer cell line panel, with mean graph midpoints (MG_MIDs) of 0.25 μM on the full panel and a GI_{50} range of 0.03−31.1 μM.

The potent antitumor activity made the class of compounds worth further evaluation, encouraging the synthesis of new [1,2]oxazolo derivatives with the aim of obtaining more potent antiproliferative agents. For a better insight into the structure−activity relationship (SAR) of the tricyclic scaffold, containing also the pyrrole moiety, we started a drug discovery program aimed at understanding the optimal structural requirements of this class of small molecules. Thus, we first identified [1,2]oxazolo[5,4-*e*]isoindole system **4**, which highlighted the potential of this group of compounds as tubulin polymerization inhibitors.[44] This class of compounds also displayed potent growth inhibitory activity on the NCI panel (GI_{50} = 0.01−27.00 μM).[44] Moreover, some derivatives significantly impaired the growth of human cancer cell lines of different histological origin, including experimental models of diffuse malignant peritoneal mesothelioma (DMPM), without interfering with normal cell proliferation. Their antiproliferative activity was found to derive from their ability to impair microtubule assembly during mitosis, with a consequent cell cycle arrest at the G2/M phase and induction of caspase-dependent apoptosis. In addition, selected derivatives, at well-tolerated doses, significantly reduced tumor volume in a DMPM xenograft model.[44,45]

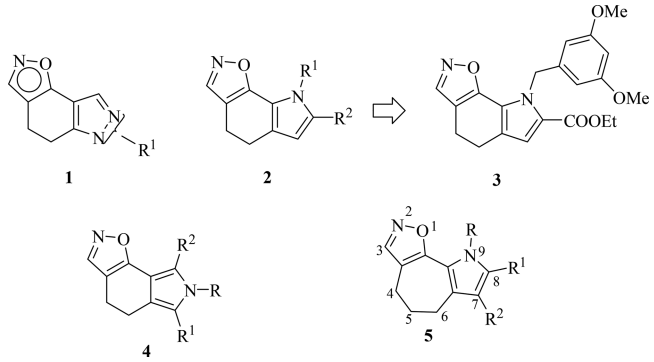

Figure 1. Structures of [1,2]oxazolo[5,4-*e*]indazoles (**1**), [1,2]-oxazolo[4,5-*g*]indoles (**2**), ethyl 8-(3,5-dimethoxybenzyl)-5,8-dihydro-4*H*-[1,2]oxazolo[4,5-*g*]indole-7-carboxylate (**3**), [1,2]oxazolo-[5,4-*e*]isoindoles (**4**), and pyrrolo[2′,3′:3,4]cyclohepta[1,2-*d*][1,2]-oxazoles (**5**).

Bearing in mind the polycyclic structure of colchicine, which includes two cyclohepta rings, and that this structural feature is recurrent in other examples reported in the literature[46,47] as potent inhibitors of tubulin assembly, we planned the expansion of the cyclohexyl central ring by one member while maintaining the [1,2]oxazole and pyrrole moieties. Thus, the new tricyclic derivatives pyrrolo[2′,3′:3,4]cyclohepta[1,2-*d*][1,2]oxazoles **5** (Figure 1) were synthesized in order to investigate the effects of this structural modification on the biological properties of these compounds. This ring system was unexplored so far as a chemical entity, and because of the close correlation with the parent structure of type **2**, in this set of derivatives we decided to retain some structural features, specifically the carboxyester and methoxy-substituted benzyl groups, that had emerged as crucial for biological activity.

CHEMISTRY

The synthetic strategy optimized by us to obtain the title ring system is outlined in Scheme 1. We started from cyclohepta-[*b*]pyrrol-8-one ketones of type **6**−**8**,[48,49] as the α position to the carbonyl is appropriate for the introduction of the second electrophilic site, essential for the subsequent cyclization with dinucleophiles.

Derivatives **7** and **8** were subjected to nitrogen functionalization with alkyl or aralkyl halides in *N*,*N*-dimethylformamide (DMF) and NaH, giving compounds **9**−**13** and **17**−**21** in 84−96% yields[48,49] and **14**−**16** and **22**−**24** in 80−90% yields. Enaminoketones **25**−**33**, useful key intermediates for the final cyclization of the [1,2]oxazole ring, were obtained by reaction of ketones **6** and **9**−**16** with an excess of *N*,*N*-dimethylformamide dimethyl acetal (DMFDMA) using DMF as solvent under microwave (MW) conditions (method C, 86−96%). Derivatives **34**−**41** can be obtained by reaction of ketones **17**−

https://dx.doi.org/10.1021/acs.jmedchem.0c01315
J. Med. Chem. 2020, 63, 12023−12042

Scheme 1. Synthesis of Pyrrolo[2′,3′:3,4]cyclohepta[1,2-*d*][1,2]oxazoles 51−76[a]

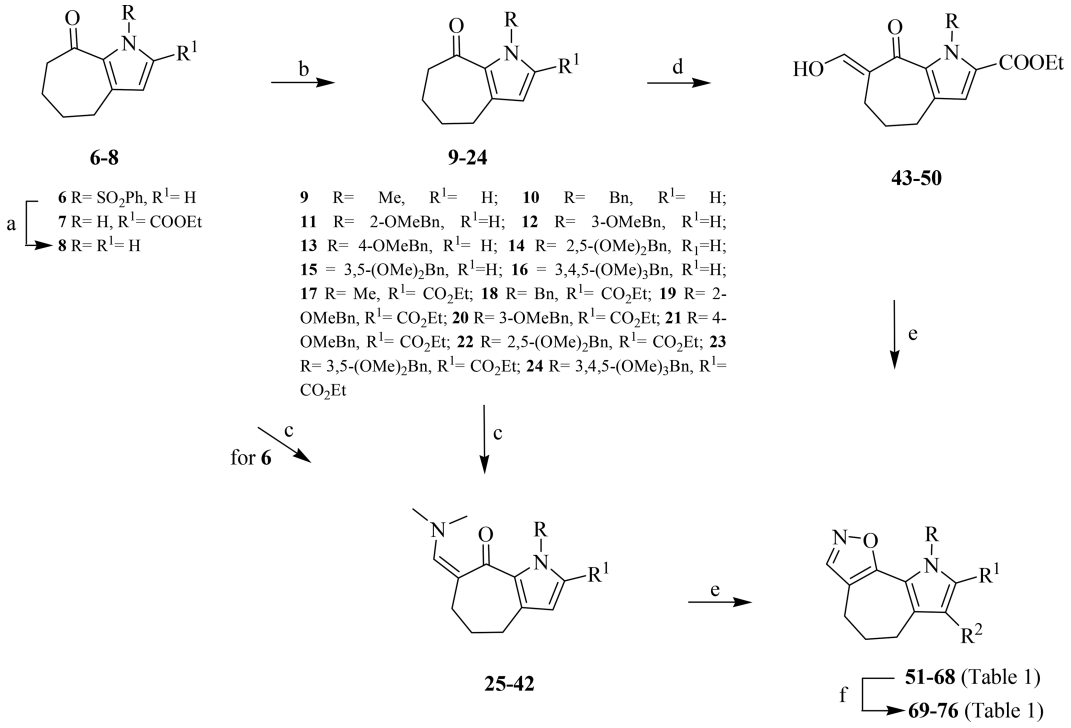

[a]Reagents and conditions: (a) NaOH, ethanol, reflux, 3 h, 80%; (b) NaH, DMF, 0 °C to rt, 1.5 h, then alkyl or aralkyl halide, 0 °C to rt, 2−24 h, 80−96%; (c) DMFDMA (1:1), DMF, MW (PW = 50 W,*T* = 100 °C), 40 min to 1.50 h, 70−87% (method A), or TBDMAM (1:1.5), DMF, MW (PW = 50 W, *T* = 100 °C), 20−40 min, 92−99% (method B), or DMFDMA (1:10), DMF, MW (PW = 150 W, *T* = 130 °C), 40 min to 2 h, 86−96% (method C); (d) *t*-BuOK, toluene, 0 °C to rt, 2 h, then HCOOEt, rt, 4 h, 60−90%; (e) $NH_2OH·HCl$, ethanol, reflux, 50 min, 60−90%; (f) *N*-chlorosuccinimide, DMF, rt, 50−75%.

24 with stoichiometric amounts of DMFDMA (method A, 70−87%) or 1.5 equiv of *tert*-butoxy bis(dimethylamino)-methane (TBDMAM) (method B, 92−99%) in DMF. Reaction of *N*-benzyl derivative **18**, belonging to the ethoxycarbonyl series, with an excess of DMFDMA led to the isolation of enaminoketone **42** (96%), in which a transesterification reaction was also observed, yielding the 2-carboxymethyl derivative.[48] Alternatively, we explored a formylation step from ketones **17**−**24**, using ethyl formate and potassium *tert*-butoxide, leading to the corresponding hydroxymethyl derivatives **43**−**50** (60−90%).

Reaction of intermediates **25**−**42** and **43**−**50** with hydroxylamine hydrochloride, as a 1,3-dinucleophile, and a stoichiometric amount of acetic acid in refluxing ethanol furnished [1,2]oxazole derivatives **51**−**68** in 60−90% yields (Table 1). Selected [1,2]oxazoles were then subjected to smooth chlorination with *N*-chlorosuccinimide to afford the corresponding chloro[1,2]oxazoles. In particular, derivatives **69**−**75**, belonging to the ethoxycarbonyl series, were obtained in good yield (60−75%). For [1,2]oxazoles **51**−**59**, which bear two pyrrole positions for potential chlorination, a mixture of the 7- and 8-halo substituted derivatives was detected by NMR analysis, and it was not possible to isolate either component as a pure compound. Only in the case of the *N*-methyl derivative **52** was the 8-chloro substituted derivative **76** (50%) recovered as a pure compound from the reaction mixture.

RESULTS AND DISCUSSION

Antiproliferative Activity in the NCI Panel. All the synthesized compounds **51**−**76** were tested at a 10^{-5} M concentration for their antitumor activity on the full NCI-60 panel comprising cancer cell lines derived from nine human cancer cell types (leukemia, non-small-cell lung, colon, central nervous system, melanoma, ovarian, renal, prostate, and breast).[50] On the basis of these results, six compounds (**62**, **63**, **66**, **67**, **70**, **75**) were selected for further screening on the same panel at five concentrations at 10-fold dilutions (10^{-4}−10^{-8} M). Almost all compounds showed antiproliferative activity against all tested human tumor cell lines, with nM to μM GI_{50} values (Table 2).

From a SAR point of view, the presence of an ethoxycarbonyl group at position 8 was crucial for activity. The most potent compound was **66**, which has a 3,5-dimethoxybenzyl substitutent at the pyrrole nitrogen and a mean graph midpoint (MG_MID) of 0.08 μM on the full NCI panel. From analysis of the GI_{50} values listed in Table 3, **66** was particularly effective against the melanoma (GI_{50} = 0.09−0.01 μM), prostate (GI_{50} = 0.04 μM), and renal (GI_{50} = 0.07−0.02 μM) cancer subpanels (Figures S1 and S2), maintaining nanomolar activity against all the tested cell lines. The calculated MG_MID value for each subpanel was 0.04 μM, much lower than the overall cell line MG_MID value. Notably, the best activity was observed for the MDA-MB-435 cell line of the melanoma subpanel, with a GI_{50} of 10 nM. Moreover, the colon and CNS cancers had mean values of 0.06 μM, again lower than the average mean value.

Compound **67**, a 3,4,5-trimethoxybenzyl substituted derivative, was the second best in potency and demonstrated high selectivity against the leukemia (GI_{50} = 0.39−0.04 μM), colon cancer (GI_{50} = 0.30−0.04 μM), CNS cancer (GI_{50} = 0.56−

https://dx.doi.org/10.1021/acs.jmedchem.0c01315
J. Med. Chem. 2020, 63, 12023−12042

Table 1. Pyrrolo[2′,3′:3,4]cyclohepta[1,2-*d*][1,2]oxazoles 51−76

[1,2]oxazole	R	R^1	R^2	yield[a] (%)
51	SO_2Ph	H	H	60
52	Me	H	H	75
53	Bn	H	H	83
54	2-OMeBn	H	H	70
55	3-OMeBn	H	H	83
56	4-OMeBn	H	H	68
57	$2,5\text{-}(OMe)_2Bn$	H	H	78
58	$3,5\text{-}(OMe)_2Bn$	H	H	76
59	$3,4,5\text{-}(OMe)_3Bn$	H	H	74
60	Me	COOEt	H	90[b],86[c]
61	Bn	COOEt	H	70[b],68[c]
62	2-OMeBn	COOEt	H	74,[b] 70[c]
63	3-OMeBn	COOEt	H	82,[b] 80[c]
64	4-OMeBn	COOEt	H	84,[b] 82[c]
65	$2,5\text{-}(OMe)_2Bn$	COOEt	H	74,[b] 72[c]
66	$3,5\text{-}(OMe)_2Bn$	COOEt	H	82,[b] 80[c]
67	$3,4,5\text{-}(OMe)_3Bn$	COOEt	H	76,[b] 75[c]
68	Bn	COOMe	H	78
69	Me	COOEt	Cl	60
70	Bn	COOEt	Cl	75
71	2-OMeBn	COOEt	Cl	74
72	3-OMeBn	COOEt	Cl	65
73	4-OMeBn	COOEt	Cl	70
74	$2,5\text{-}(OMe)_2Bn$	COOEt	Cl	68
75	$3,5\text{-}(OMe)_2Bn$	COOEt	Cl	70
76	Me	Cl	H	50

[a]Values represent the yield obtained at the final reaction step. [b]These yields were obtained starting from (dimethylamino)methylidene ketones **34−41**. [c]These yields were obtained starting from hydroxymethylidene ketones **43−50**.

Table 2. Overview of the Results of the NCI *in Vitro* Human Tumor Cell Line Screening for Derivatives 62, 63, 66, 67, 70, 75

compd	N^a	N^b	$GI_{50}{}^c$	MG_MID[d]
62	56	50	0.30−46.2	4.47
63	56	56	0.15−18.7	1.45
66	56	55	0.01−13.4	0.08
67	55	55	0.01−64.9	0.20
70	55	46	1.29−5.89	7.08
75	57	57	0.03−27.0	0.41

[a]Number of cell lines investigated. [b]Number of cell lines giving positive GI_{50} values. [c]GI_{50} = concentration that inhibits 50% net cell growth (μM). [d]MG_MID = mean graph midpoint (μM); the arithmetic mean value for all tested cancer cell lines. If the indicated effect was not attainable under the concentration range used, the highest tested concentration was used for the calculation.

0.07 μM), melanoma (GI_{50} = 0.41−0.02 μM), ovarian cancer (GI_{50} = 0.72−0.03 μM), and breast cancer (GI_{50} = 0.74−0.04 μM) subpanels, with GI_{50} values at submicromolar to nanomolar levels (Figures S3 and S4). Isoxazole **67**, even if it was 1 order of magnitude less potent than the dimethoxy substituted analogue **66**, reached nanomolar GI_{50} values in each subpanel, and it also had a 10 nM GI_{50} against the NCI-H522 non-small-cell lung cancer cells.

Overall, the presence of a methoxy group at position 4 of the 3,5-dimethoxybenzyl substituent caused a significant loss of activity (compare **66**, MG_MID = 0.08 μM, with **67**, MG_MID = 0.20 μM), while removal of one methoxy group (**62**, MG_MID = 4.47 μM; **63**, MG_MID = 1.45 μM) produced an even larger (up to 2 logs) decrease in activity. Introduction of chlorine in the 7 position generally reduced activity relative to the corresponding parent compound (compare **66**, MG_MID = 0.08 μM, with **75**, MG_MID = 0.41 μM). In contrast, the reverse was observed for **70**, which is more effective than the parent compound **61**.

Compared to the previously reported classes of compounds,[43] pyrrolo[2′,3′:3,4]cyclohepta[1,2-*d*][1,2]oxazoles had strong antiproliferative effect with a 3-fold improvement in overall activity on the NCI panel. The 3,5-dimethoxybenzyl and the ethoxycarbonyl functionalities were preferred substituents for this activity, as was the case with the parent cyclohexyl analogues **2**. Although [1,2]oxazoloisoindoles represent positional isomers, the same substitutions yielded ineffective compounds, thus indicating the high correlation between the pyrrolo[2′,3′:3,4]cyclohepta[1,2-*d*][1,2]oxazole **5** and the [1,2]oxazolo[4,5-*g*]indole system **2**.

Screening Results in Lymphoma Models. All compounds were further tested at the concentration of 1 μM on four cell lines derived from distinct lymphoma histotypes, plus two with secondary resistance to the PI3Kδ inhibitor idelalisib[51] or to the BTK inhibitor ibrutinib.[52] After a 72 h incubation, compounds **57**, **66**, **67**, **71**, **74**, and **75** showed potent growth inhibitory effects against all tested cell lines, with the percentage of proliferating cells reduced to 9−60% of the untreated cells (Table 4). For comparison, the same experiments were conducted using compound **3**, but the response to it was minimal, and thus it was not considered further.

Compounds showing some activity, plus compound **70** based on the NCI panel data, were tested with a wider range of concentrations. Some presented potent growth growth inhibitory effects on some or all of the lymphoma cell lines, with IC_{50} values lower than 500 nM (Table 5).

Effects of Test Compounds in Human Peripheral Blood Lymphocytes (PBLs). To obtain an initial idea of whether the compounds described here had activity against normal cells, **63**, **66**, and **75** were examined for cytotoxicty against PBLs from healthy donors. As shown in Table 6, these three compounds were practically devoid of any activity both in quiescent and in lymphocytes induced to proliferate by the mitogenic stimulus phytohematoaglutinin (PHA). In all cases, we obtained a GI_{50} > 100 μM, demonstrating low toxicity for these healthy human cells.

In this context, we point out that in other studies other molecules that bind in the colchicine site were shown to have low toxicity toward lymphocytes from healthy subjects.[53−56] Although at present the reason for this low toxicity is unclear, it is nevertheless interesting that even healthy lymphocytes induced to actively replicate with a mitogenic stimulus respond in the same way as quiescent lymphocytes.

Tubulin Assays. To assess if pyrrolocyclohepta[1,2]-oxazoles were able to bind to tubulin, seven compounds (Table 7) were tested for their antitubulin activity in comparison with reference compound CA-4, which potently inhibits both tubulin assembly and colchicine binding to tubulin.[57] Moreover, compound **3** was also evaluated as a comparison between the two scaffolds.

The colchicine assay was performed on compounds that yielded IC_{50} values of <6 μM in the assembly assay. Reaction mixtures in the assembly assay contained 9 μM (0.9 mg/mL)

https://dx.doi.org/10.1021/acs.jmedchem.0c01315
J. Med. Chem. 2020, 63, 12023−12042

Table 3. *In Vitro* GI_{50} (μM) Values of Compounds 62, 63, 66, 67, 70, and 75 in Individual Tumor Cell Lines

cell line	62	63	66	67	70	75	cell line	62	63	66	67	70	75
Leukemia							M14	3.67	0.54	0.05	0.15	3.78	0.26
CCRF-CEM	2.87	2.17	0.05	0.30	2.21	0.25	MDA-MB-435	0.35	0.15	0.01	0.02	1.40	0.03
HL-60(TB)	3.04	0.53	0.03	0.19	3.32	0.31	SK-MEL-2	-	0.56	0.04	-	-	0.22
K-562	1.59	0.39	0.04	0.13	3.68	0.29	SK-MEL-28	>100	5.12	0.09	0.30	-	0.66
MOLT-4	5.68	2.30	0.26	0.39	3.58	0.58	SK-MEL-5	2.61	0.75	0.04	0.17	3.53	0.49
RPMI-8226	4.11	1.89	0.05	0.38	3.27	0.39	UACC-257	-	7.61	-	-	-	-
SR	0.43	0.28	0.03	0.04	1.80	0.07	UACC-62	3.37	0.51	0.07	0.05	4.01	0.11
Non-Small-Cell Lung Cancer							**Ovarian Cancer**						
A549/ATCC	-	0.76	0.06	-	-	-	IGROV1	1.99	1.16	0.06	0.06	4.39	0.34
EKVX	-	-	-	-	-	-	OVCAR-3	0.87	0.30	0.02	0.03	3.13	0.19
HOP-62	1.89	4.34	-	0.17	4.35	0.29	OVCAR-4	9.35	18.7	13.4	0.72	-	0.85
HOP-92	0.30	4.21	-	-	-	0.46	OVCAR-5	>100	5.94	0.18	0.53	>100	-
NCI-H226	>100	21.0	7.98	1.21	>100	9.71	OVCAR-8	3.85	3.13	0.08	0.24	-	0.41
NCI-H23	8.52	-	-	0.37	-	0.68	NCI/ADR-RES	1.36	0.43	0.03	0.06	2.83	0.20
NCI-H322M	5.23	-	-	0.32	>100	0.51	SK-OV-3	2.70	2.83	0.05	0.13	>100	0.24
NCI-H460	3.88	3.53	0.04	0.23	3.62	0.35	**Renal Cancer**						
NCI-H522	0.35	0.23	0.02	0.01	1.29	0.03	786−0	>100	6.74	0.05	0.97	-	4.24
Colon Cancer							A498	3.46	0.44	0.02	0.11	4.38	0.17
COLO 205	0.87	0.58	0.03	0.04	3.53	0.17	ACHN	16.6	3.40	0.06	0.29	5.89	0.94
HCC-2998	>100	4.18	0.23	0.30	-	-	CAKI-1	3.51	2.31	0.05	0.07	3.51	0.28
HCT-116	3.79	0.47	0.04	0.19	4.02	0.43	RXF 393	2.08	0.67	0.02	0.12	-	0.25
HCT-15	2.24	0.45	0.04	0.16	3.39	0.37	SN12C	>100	3.51	0.07	0.76	-	0.83
HT29	0.91	0.36	0.03	0.07	2.95	0.27	TK-10	67.8	11.2	>100	64.9	>100	10.3
KM12	2.10	0.46	0.03	0.05	3.70	0.32	UO-31	6.53	3.37	0.05	0.08	-	0.78
SW-620	2.02	0.48	0.04	0.14	3.81	0.32	**Prostate Cancer**						
CNS Cancer							PC-3	2.48	2.35	0.04	0.17	3.16	0.29
SF-268	46.2	6.71	0.05	0.52	>100	1.91	DU-145	5.27	2.18	0.04	0.28	>100	0.35
SF-295	1.38	0.62	0.03	0.44	>100	0.06	**Breast Cancer**						
SF-539	2.48	1.14	0.03	0.12	-	0.24	MCF7	0.71	0.37	0.03	0.04	3.21	0.10
SNB-19	64.7	8.23	0.15	0.56	>100	0.52	MDA-MB-231/ATCC	9.12	1.84	0.24	0.48	3.51	0.84
SNB-75	1.97	1.60	0.03	0.07	-	0.22	HS 578T	3.38	1.60	0.04	0.34	-	0.45
U251	3.78	-	-	0.14	-	0.31	BT-549	7.73	0.98	1.72	0.29	-	27.0
Melanoma							T-47D	2.46	2.00	-	0.10	2.69	0.44
LOX IMVI	7.64	1.75	0.05	0.41	5.26	0.88	MDA-MB-468	2.95	0.34	0.03	0.74	-	0.73
MALME-3M	3.08	0.89	-	0.05	3.68	0.20							

tubulin in the assembly assay, and in the colchicine assay they contained 0.5 μM tubulin, 5.0 μM [^{3}H]colchicine, and 5.0 μM inhibitor.

In the assembly assay, three compounds had IC_{50} values of >6 μM. These were compounds **3**, **56**, and **63**. In addition, we examined several other compounds shown in Table 1, and they were uniformly minimally active in the tubulin assembly assay. The five other compounds (**57**, **58**, **66**, **67**, and **75**) were more active in the assembly assay, with **66** and **75** the most active, with IC_{50} values of 2.6 and 1.9 μM, respectively. A value of 1.2 μM was obtained for CA-4. The five pyrrolocyclohepta[1,2]-oxazoles most active as assembly inhibitors inhibited colchicine binding by 25−62% versus 97% for CA-4. Overall, the most powerful compound was **66**, which inhibited tubulin polymerization with an IC_{50} of 2.6 μM and displayed 62% inhibition of colchicine binding. No compound was as active as CA-4 in any assay.

The effects of compounds **66** and **75** on tubulin assembly are shown in Figure 2, panels A and B, respectively. These data were obtained in computer-driven recording spectrophotometers equipped with electronic temperature controllers that rapidly change the temperature in the reaction mixtures in the cuvettes. The assembly reaction was measured by following turbidity development at 350 nM. After a minute's equilibration at 0 °C, the temperature was jumped to 30 °C and assembly was followed for 20 min. At 21 min, the temperature was jumped backward to 0 °C, and the reaction mixtures were followed for another 8 min. Several compound concentrations were evaluated in each experimental sequence, and the IC_{50} for inhibition of turbidity development was defined as the compound concentration, obtained by interpolation, that inhibited the extent of turbidity development by 50% after 20 min at 30 °C. The 30−0 °C transition was included to distinguish inhibition of microtubule assembly from aberrant assembly reactions induced by numerous compounds. Typically, the aberrant assembly reaction products either are cold stable or have different temperature stability properties as compared to microtubules.

Molecular Modeling. Compound **3** and all the compounds belonging to the new class of pyrrolo[2′,3′:3,4]-cyclohepta[1,2-*d*][1,2]oxazoles **5** were docked into the colchicine and vinblastine binding sites, by selecting for each of them the pose with the best G-Score (kcal/mol). A better affinity for the colchicine site (Table S2) was observed for all ligands, further confirming their specificity for this binding pocket. Moreover, most of the newly synthesized compounds had a better affinity than the parent compound **3**.

https://dx.doi.org/10.1021/acs.jmedchem.0c01315
J. Med. Chem. 2020, 63, 12023−12042

Table 4. Proliferating Cells (%) after Treatment with the Indicated Pyrrolocyclohepta[1,2-*d*][1,2]oxazoles[a]

compd	VL51 (MZL)	VL51 idelalisib-resistant	VL51 ibrutinib-resistant	MINO (MCL)	HBL1 (ABC DLBCL)	SU-DHL-10 (GCB DLBCL)
3	93.5	106.9	123.1	94.5	95.6	80.0
51	88.1	118.2	120.8	104.5	118.1	110.2
52	87.4	106.7	100.3	104.3	101.4	70.2
53	103.1	128.0	125.0	109.3	108.9	70.2
54	119.9	135.7	112.0	112.1	122.2	141.4
55	112.3	133.0	124.6	115.2	127.3	80.3
56	110.3	126.8	109.8	108.9	123.0	74.6
57	36.5	34.3	37.0	8.5	29.6	11.0
58	84.0	78.4	73.0	101.4	113.6	72.4
59	97.6	111.5	92.1	99.0	114.0	94.6
60	107.7	115.2	125.0	111.5	146.2	61.7
61	93.3	116.8	117.7	106.3	123.9	65.2
62	71.3	63.6	80.3	103.8	127.6	51.1
63	66.7	62.3	64.9	86.3	117.1	51.5
64	87.4	116.4	102.0	112.3	125.1	66.3
65	86.2	96.4	94.0	107.0	111.0	71.6
66	40.1	34.3	40.5	9.1	24.1	11.3
67	40.5	36.6	40.4	8.9	24.2	11.2
68	94.5	122.7	120.4	98.8	109.1	78.9
69	93.8	121.4	109.7	115.9	102.6	78.5
70	108.1	111.4	104.4	104.1	104.2	69.5
71	58.8	52.2	56.2	55.9	97.0	58.2
72	106.8	127.8	102.9	110.2	105.1	76.9
73	113.3	126.2	101.5	99.5	106.9	87.4
74	40.4	37.7	44.4	9.8	29.0	13.3
75	38.1	40.2	40.8	9.5	20.7	11.5

[a]MZL indicates marginal zone lymphoma; MCL indicates mantle cell lymphoma; ABC DLBCL indicates activated B-cell-like diffuse large B cell lymphoma; and GCB DLBCL indicates germinal center B-cell type diffuse large B cell lymphoma.

Table 5. IC_{50} (μM) Values of Selected Pyrrolocyclohepta[1,2-*d*][1,2]oxazoles[a]

compd	VL51 (MZL)	MINO (MCL)	HBL1 (ABC DLBCL)	SU-DHL-10 (GCB DLBCL)
62	3.2	4	>5	3.6
63	2.3	2.6	>5	3
66	0.25	0.25	0.3	0.25
67	0.5	0.6	0.9	0.6
57	0.2	0.4	0.6	0.3
70	>10	>10	>10	9
71	2.4	3.4	>5	2.2
74	0.5	0.8	1	0.7
75	0.8	0.9	0.9	0.9

[a]MZL indicates marginal zone lymphoma; MCL indicates mantle cell lymphoma; ABC DLBCL indicates activated B-cell-like diffuse large B cell lymphoma; and GCB DLBCL indicates germinal center B-cell type diffuse large B cell lymphoma.

Table 6. Cytotoxicity of Compounds for Human Peripheral Blood Lymphocytes

	GI_{50} (μM)[a]	
compd	$PBL_{resting}$[b]	PBL_{PHA}[c]
63	>100	>100
66	>100	>100
75	>100	>100
vincristine	7.5 ± 3.1	1.2 ± 0.6

[a]Compound concentration required to inhibit cell growth by 50%. Values are the mean ± SEM for three separate experiments. [b]PBLs not stimulated with PHA. [c]PBLs stimulated with PHA.

Table 7. Inhibition of Tubulin Assembly and Colchicine Binding by Compounds 56, 57, 58, 63, 66, 67, and 75

	inhibition of tubulin assembly	inhibition of colchicine binding
compd	IC_{50} ± SD (μM)	% inhibition ± SD 5 μM inhibitor
CA-4	1.2 ± 0.08	97 ± 0.9
3	9.2 ± 0.4	
56	8.2 ± 0.5	
57	3.2 ± 0.06	38 ± 0.7
58	5.7 ± 1	25 ± 3
63	6.3 ± 0.06	
66	2.6 ± 0.03	62 ± 2
67	4.6 ± 0.8	25 ± 0.01
75	1.9 ± 0.1	42 ± 5

To further investigate the binding mode of the best active compounds (**57**, **58**, **63**, **66**, **67**, and **75**) in the biological assays with respect to **3**, molecular modeling studies were performed on the 3N2G model, which displays two additional neighboring pockets (zones 2 and 3) in the tubulin colchicine domain. As was the case with their parent compound **3**, compounds **57**, **58**, **63**, **66**, **67**, and **75** had a better G-Score toward the main site (zone 1) of the colchicine domain (Table S3). As shown in Figure S5, our compounds had unfavorable steric contacts with an additional hydrophobic pocket of the β subunit, formed by residues E200, L255, A316, A317, A354, C241, and T179.

On the other hand, the best docking poses of active compounds with tubulin structure 4O2B, containing zones 1 and 2 of the colchicine site, showed strong hydrophobic

https://dx.doi.org/10.1021/acs.jmedchem.0c01315
J. Med. Chem. 2020, 63, 12023−12042

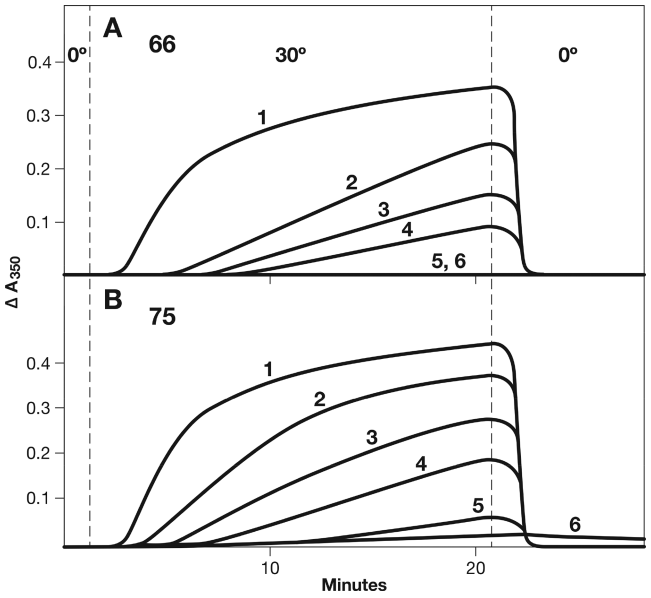

Figure 2. Inhibition of tubulin assembly by **66** (A) and **75** (B). Reaction mixtures (0.25 mL, final volume) contained 0.8 M monosodium glutamate (adjusted to pH 6.6 in a 2 M stock solution), 0.9 μM (0.9 mg/mL) tubulin, 4% dimethyl sulfoxide, compounds at the indicated concentrations, and following a 15 min preincubation in 0.24 mL, 0.2 mM GTP (added in a 10 μL volume). The reaction mixtures, following the preincubation, were kept on ice and transferred to cuvettes held at 0 °C in a recording spectrophotometer. After baselines were established, the reactions were initiated. At 1 min, the electronic temperature controller automatically increased the temperatures in the cuvettes to 30 °C, and at 21 min, the temperatures in the cuvettes were returned to 0 °C (the temperature transitions take about 30 and 60 s, respectively). (A) The reaction mixtures contained the following concentrations of compound **66**: curve 1, none; curve 2, 2.0 μM; curve 3, 3.0 μM; curve 4, 4.0 μM; curve 5, 5.0 μM; curve 6, 7.5 μM. (B) The reaction mixtures contained the following concentrations of compound **75**: curve 1, none; curve 2, 1.0 μM; curve 3, 1.5 μM; curve 4, 2.0 μM; curve 5, 3.0 μM; curve 6, 4.0 μM.

interactions with β-tubulin residues L248, A250, A354, I318, A316, and L255 (Figure 3). In particular, **66** and **75**, which are the compounds with the best biological activity, displayed a binding geometry similar to that of colchicine in zones 1 and 2 of the pocket, by directing their methoxybenzyl groups toward the C241 residue (Figure 3D and Figure 3F). Moreover, **75** also established a halogen bond between its chlorine and the backbone of V181 and an H-bond between the oxazole moiety and the backbone of N249. Conversely, compound **3** and the less active compounds (**57**, **58**, **63**, and **67**) showed a different binding orientation, with the tricyclic portion steered toward residue C241 (Figure 3A,B,C,E,G).

In particular, for compound **3** we observed a π−cation between its pyrrole and β-tubulin K352, while hydrophobic interactions were much weaker than with the other derivatives.

The best docking poses of **57**, **58**, **63**, **66**, **67**, **75**, and **3** against the 4O2B model were submitted to explicit water solvent molecular dynamics (MD) simulations, with the aims to add depth to our analysis and to investigate the possibility of induced-fit phenomena in the tubulin recognition process of our ligands. As a reference, the X-ray model of 4O2B, containing colchicine in its binding pocket, was included in similar calculations. In the Supporting Information we reported the geometric behavior of all MD simulations and the analysis of their most representative structures, by computing the related binding free energy and the global number of contacts (Table S4).

With the respect to its docking pose (Figure 3G), the most representative MD structure of **3** showed the establishment of three H-bonds (Figure 4G). In particular, the two methoxy groups interact with β-tubulin N101 and N249, while the carbonyl group establishes an H-bond with S318. However, the formation of these hydrogen bonds does not allow stability of the bonding mode and does not bring about an energy gain, due to the lower ability to establish hydrophobic interactions.

Regarding **66**, the most representative MD structure showed that the tubulin molecule adjusted its residues to allow establishment of an H-bond between its methoxy group and the side chain of C241 and to permit a π−cation between its oxazole ring and K254 (Figure 3D). Further hydrophobic interactions with β-tubulin K254, A250, L255, A316, and A354 stabilized the complex. Likewise, **75** showed a binding mode similar to that of **66**, by engaging an H-bond between its 4-

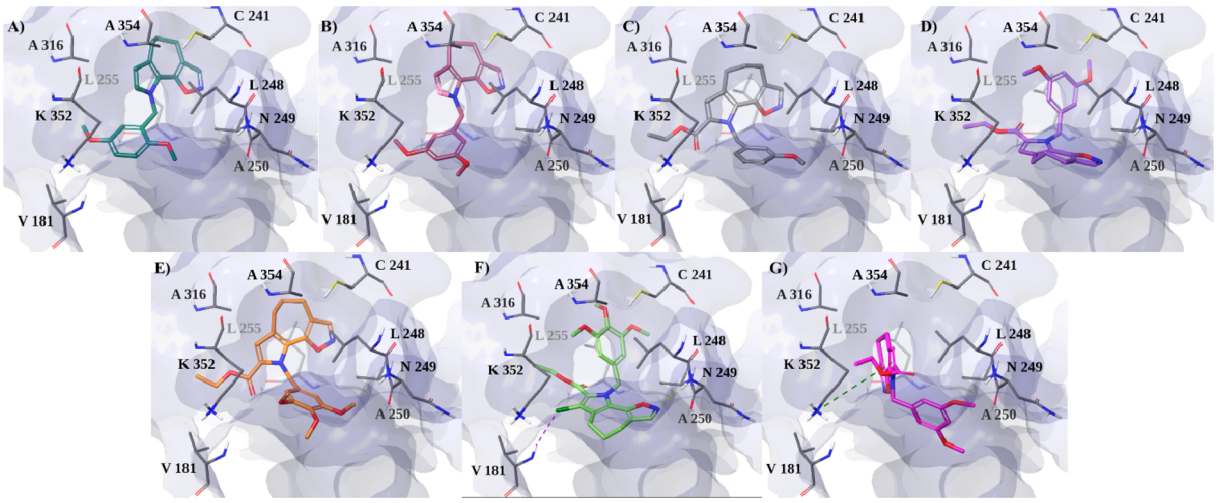

Figure 3. Best docked poses of (A) **57**, (B) **58**, (C) **63**, (D) **66**, (E) **67**, (F) **75**, and (G) **3** with the 4O2B crystal structure of tubulin, depicting zones 1 and 2 of the colchicine site. Tubulin is shown in a faded blue surface, while ligands and residues, involved in the most important interactions, are shown as sticks. Halogen bond and π−cation interactions are indicated as dashed violet and dark-green lines, respectively.

https://dx.doi.org/10.1021/acs.jmedchem.0c01315
J. Med. Chem. 2020, 63, 12023−12042

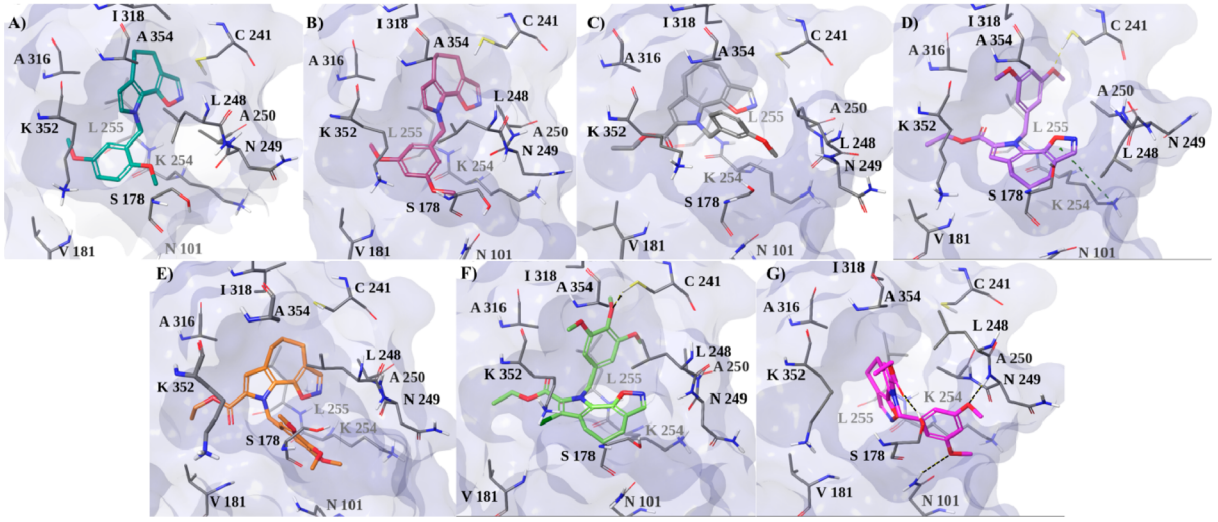

Figure 4. Most representative MD structure of tubulin (PDB code 4O2B) complexed with (A) **57**, (B) **58**, (C) **63**, (D) **66**, (E) **67**, (F) **75**, and (G) **3**. Tubulin is depicted as a pale blue surface, and ligands and residues with the most critical interactions are in stick format. Hydrogen bond and π−cation interactions are indicated as dashed black and dark-green lines, respectively.

methoxy group and C241 and several hydrophobic interactions with L248, A250, L255, I318, and A354 (Figure 4F). With respect to its docking pose (Figure 3F), we observed the absence of the halogen bond and the H-bond with N249, both of which can be considered useful interactions in the recognition process but not in complex stabilization. In fact, although **67** and **75** differ only by the chlorine atom, the docking simulation proposed different binding poses for them. Thus, the absence of chlorine seems responsible for the different orientation of **67** in the tubulin pocket, preventing also the establishment of the H-bond with C241 during MDs (Figure 4E), which seems very important for the stabilization of the most active compounds. Finally, during MDs **57** and **58** increased their hydrophobic interactions with the L255, A316, I318, K352, and A354 residues (Figure 4A,B).

In conclusion, compared to the parent molecule **3**, the most active compounds of the new class of pyrrolo[2′,3′:3,4]-cyclohepta[1,2-*d*][1,2]oxazoles displayed an improved interaction with tubulin because of the greater contribution of the lipophilic energy components. Moreover, **66** and **75** showed a peculiar binding mode, characterized by the methoxybenzyl portion placed similarly to colchicine.

Compounds 63, 66, and 75 Induced Mitotic Arrest of the Cell Cycle. To evaluate the effects of compounds **63**, **66**, and **75** on cell cycle progression, we first treated HeLa cells for 24 h.The cells were then labeled with propidium iodide (PI) and analyzed by flow cytometry. As shown in Figure 5 (panel B), compound **66** induced arrest of the cell cycle in the G2/M phase. This effect occurred in a concentration-dependent manner, and partial arrest in G2/M occurred at the lowest concentration examined (0.125 μM), while at the highest concentration (0.5 μM) over 80% of the cells were arrested in G2/M. Compound **75** (panel C) exhibited a similar behavior, although the first appearance of G2/M arrest occurred at 0.25 μM. Only modest activity was observed with compound **63** (panel A), as the metaphase arrest occurred only at the highest concentration (1 μM) examined, as compared to the other two compounds, and furthermore, at this concentration there was only a slight reduction in the proportion of S phase cells observed.

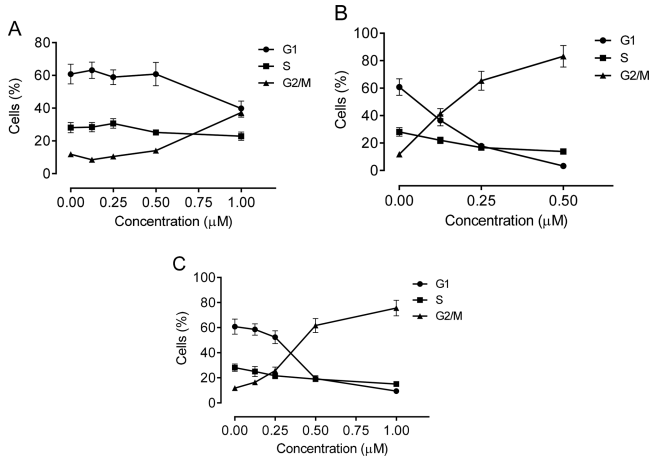

Figure 5. Percentage distribution in the three phases of the cell cycle of HeLa cells treated with **63** (A), **66** (B), or**75** (C) at the indicated concentrations for 24 h. Cells were analyzed by flow cytometry after labeling with PI as described in the Experimental Section. Data are presented as the mean ± SEM of three experiments.

Compound 66 Induced Alteration of Cell Cycle Checkpoint Proteins. We studied the effects of **66** on the expression of various checkpoint proteins that play roles in cell cycle regulation. Cells that enter mitosis do so through the involvement of cyclin B1 complexed to cdc2. This complex is activated through the dephosphorylation of phospho-cdc2, which is a cdc25c-dependent process that ultimately leads to the phosphorylation of cyclin B1. This phosphorylated enzyme triggers cells to enter mitosis.[58,59]

Figure 6 demonstrates a substantial increase of cyclin B1 expression after a 24 h treatment with 0.5 μM **66**. In contrast, total cdc25c expression was strongly reduced, and in good agreement, the expression of phosphorylated cdc2 was strongly decreased after both 24 and 48 h. Dephosphorylation of this protein is needed to activate the cdc2/cyclin B complex, and this effect is stimulated by cdc25c.[58,59]

These data demonstrate that cdc2/cyclin B1 complexes were not activated, thus blocking cells from exiting mitosis and leading to apoptotic cell death.

https://dx.doi.org/10.1021/acs.jmedchem.0c01315
J. Med. Chem. 2020, 63, 12023−12042

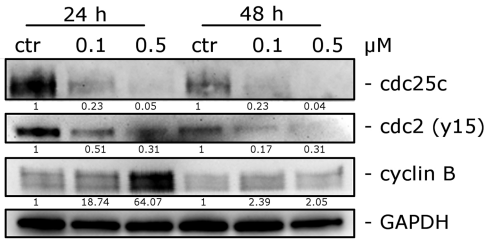

Figure 6. Effects of **66** on G2/M checkpoint proteins. HeLa cells were treated with 0.1 or 0.5 μM compound **66** for 24 or 48 h. The cells were harvested and lysed for the detection of cdc25c, p-cdc2^{Y15}, and cyclin B expression by Western blot analysis. To confirm equal protein loading, each membrane was stripped and reprobed with anti-GAPDH antibody. The relative expression of proteins was analyzed by scanning densitometry using ImageJ software and reported as a ratio protein/GAPDH.

Compound 66 Induced Apoptosis. To analyze the mode of cell death induced by compound **66** in HeLa cells, we utilized a double labeling assay of the cells with annexin-V and PI. This procedure, through a flow cytometric analysis, distinguishes four different cell populations: live cells (annexin-V$^-$/PI$^-$), early apoptotic cells (annexin-V$^+$/PI$^-$), late apoptotic cells (annexin-V$^+$/PI$^+$), and necrotic cells (annexin-V$^-$/PI$^+$).

As Figure 7 denonstrates, HeLa cells treated with **66** showed a significant increase in apoptotic cells after a 24 h treatment at

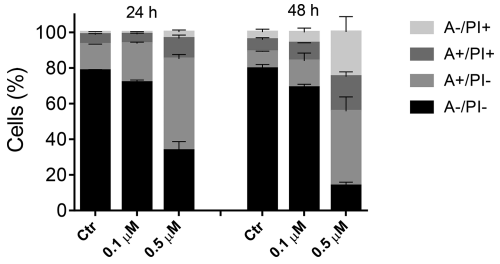

Figure 7. Flow cytometric analysis of apoptotic cells after treatment of HeLa cells with **66** at the indicated concentrations after incubation for 24 or 48 h. The cells were harvested and labeled with annexin-V-FITC and PI and analyzed by flow cytometry. Data are represented as the mean ± SEM of three independent experiments.

0.5 μM. The percentage of apoptotic cells increased further after 48 h, when there was a substantial increase in necrotic cells, indicating that the compound ultimately induced cell death by necrosis as well as apoptosis.

Compound 66 Induced Apoptosis through the Mitochondrial Pathway. In the initial stages of induction of apoptosis, the mitochondrial transmembrane potential ($\Delta\psi_{mt}$) is altered and leads to to a reduction of $\Delta\psi_{mt}$ and release of cytochrome c into the cytoplasm.[60,61] Moreover, this effect occurs with many antimitotic agents and in a variety of cell lines.[62−64] As shown in Figure 8 (panel A), compound **66** at both concentrations used (0.1 and 0.5 μM) induced in a time- and concentration-dependent manner a significant increase in the percentage of cells with low $\Delta\psi_{mt}$.

One consequence of mitochondrial depolarization caused by the release of cytochrome *c* into the cytoplasm is the increase in reactive oxygen species (ROS).[65] Therefore, we wanted to evaluate whether ROS production increased following treatment with compound **66**. To do this, we used the fluorescent

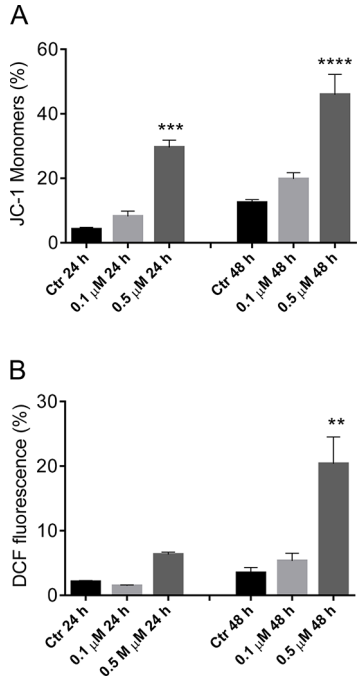

Figure 8. Evaluation of mitochondrial membrane potential ($\Delta\psi_{mt}$) and ROS production after treatment of HeLa cells with compound **66** (panels A and B, respectively). Cells were treated with the indicated concentration of compound for 24 or 48 h and then stained with the fluorescent probe JC-1 (A) or H_2-DCFDA as described in the Experimental Section. Data are presented as the mean ± SEM of three independent experiments: $^{**}p < 0.01$, $^{***}p < 0.001$, $^{****}p < 0.0001$ vs control.

probe 2,7-dichlorodihydrofluorescein diacetate (H_2-DCFDA), which is oxidized to the fluorescent compound dichlorofluorescein (DCF) upon ROS production. The results of the cytofluorimetric analysis are presented in Figure 8 (panel B), which demonstrates that **66** induced the production of ROS in HeLa cells after a 48 h treatment at 0.5 μM, in agreement with the reduction of $\Delta\psi_{mt}$. Note that the increase in ROS is only detectable after mitochondrial depolarization, indicating that ROS production results from mitochondrial damage.

Compound 66 Induced PARP Cleavage and Reduced the Expression of Mcl-1 and XIAP Proteins. To study in greater detail the apoptotic process induced by **66**, we evaluated the expression of the cleaved fragment of poly-(ADP)ribose polymerase (PARP), a common marker of apoptosis,[66] by Western blot analysis. HeLa cells were treated with compound **66** at 0.1 or 0.5 μM for 24 or 48 h. The cleavage fragment of PARP appeared at 24 h after beginning treatment with only 0.1 μM **66**. The expression of two antiapoptotic proteins, Mcl-1 and XIAP, was also studied. Mcl-1, a member of the Bcl-2 family, is highly expressed in many types of tumors and takes part in the apoptotic response to multiple stimuli. Specifically, sensitivity to antimitotic drugs is regulated by Mcl-1 levels,[67,68] and we found that compound **66** treatment of HeLa cells resulted in a reduction in Mcl-1 levels (Figure 9). Similarly, expression of Xiap, a member of the family of inhibitors of apoptosis proteins, was reduced (at 24 h) and diappeared (at 48 h) after HeLa cell treatment with **66** (Figure 9). The functions of this protein are to inhibit the activity of caspase-3, caspase-7, and caspase-9 through a direct interaction with these enzymes. Following this interaction, the entire apoptotic process is inhibited.[69] Thus, treatment of

https://dx.doi.org/10.1021/acs.jmedchem.0c01315
J. Med. Chem. 2020, 63, 12023−12042

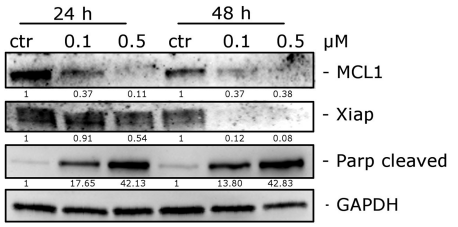

Figure 9. Western blot analysis of Mcl-1 XIAP and PARP after treatment of HeLa cells with **66** at the indicated concentrations and for the indicated times. To confirm equal protein loading, each membrane was stripped and reprobed with anti-GAPDH antibody. The relative expression of proteins was analyzed by scanning densitometry using ImageJ software and reported as a ratio protein/GAPDH.

HeLa cells with **66** resulted in downregulation of Mcl-1 and Xiap and impairment of their antiapoptotic functions.

CONCLUSIONS

Among anticancer agents, colchicine site inhibitors still attract much attention in medicinal chemistry because of their potential to overcome disadvantages encountered by other antitubulin agents binding at other sites. Our study indicates that pyrrolo[2′,3′:3,4]cyclohepta[1,2-*d*][1,2]oxazoles can be considered a novel class of antimitotic compounds binding at the colchicine site, with antitumor activity in multiple cancer cell lines and with improved features with respect to the previously identified cyclohexyl analogue **3**.

We show here that expanding the central ring to seven members, in part to mimic the seven-member rings of colchicine, resulted in enhanced antiproliferative activities in multiple cell lines. This was based on increased antitubulin activity, which in turn caused cell cycle arrest at G2/M, with resultant apoptosis. Molecular modeling rationalized the improvement in activity by central ring expansion, probably caused by an improvement in binding affinity for the colchicine binding pocket because of a greater contribution of the lipophilic energy components.

Among these compounds, five derivatives (**62**, **63**, **66**, **67**, and **75**) showed promising antiproliferative effects, and in particular, **66** and **67**, bearing a methoxysubstituted *N*-benzyl moiety and an ethoxycarbonyl group, reached nanomolar growth inhibitory effects against solid and liquid tumor cells and submicromolar activity against lymphoma cell lines. Their mechanism of action is probably through inhibition of tubulin assembly by binding in the colchicine site, and this mechanism was particularly marked for **66**, which inhibited tubulin polymerization with an IC_{50} of 2.6 μM and inhibited colchicine binding by 62% under the conditions examined.

Investigation of the mechanism of action showed the ability of the new [1,2]oxazoles to impair cell cycle progression and induce apoptosis through the mitochondrial pathway. The most active compound **66** was able to arrest HeLa cells in the G2/M phase of the cell cycle in a concentration dependent manner. This effect was accompanied by apoptosis, mitochondrial depolarization, generation of ROS, and activation of PARP cleavage. These results indicate that the cellular actions of these agents involved mitotic arrest, due to interference with the functions of the mitotic spindle, and an apoptotic cell death. Taken together, the biological results collected so far indicate that our class of [1,2]oxazoles might find an important place in the set of molecules of interest for the development of pharmaceutical strategies against cancer. Further evolution of this class in terms of ADMET profile will be considered to establish the best trade-off between biological activity and drug-like properties for further preclinical studies.

EXPERIMENTAL SECTION

Chemistry. *Synthesis and Characterization.* MW irradiation was performed using a CEM Discover Labmate apparatus. All melting points were taken on a Büchi melting point M-560 apparatus. IR spectra were determined in bromoform with a Shimadzu FT/IR 8400S spectrophotometer. ^{1}H and ^{13}C NMR spectra were measured at 200 and 50.0 MHz, respectively, in DMSO-d_6 or $CDCl_3$ solution using a Bruker Avance II series 200 MHz spectrometer. Column chromatography was performed with Merck silica gel (230−400 mesh ASTM) or a Büchi Sepacor chromatography module (prepacked cartridge system). Elemental analyses (C, H, N) were within ±0.4% of theoretical values and were performed with a VARIO EL III elemental analyzer. The purity of all the tested compounds was >95%, determined by HPLC (Agilent 1100 series).

Compounds **6**−**13**, **17**−**21**, **25**−**30**, **34**−**38**, and **42** were prepared according to our published procedures.[48,49]

*General Procedure for the Preparation of 1-Substituted-4,5,6,7-tetrahydrocyclohepta[b]pyrrol-8(1H)-one (**14**−**16**) and Ethyl 1-Substituted-8-oxo-1,4,5,6,7,8-hexahydrocyclohepta[b]pyrrole-2-carboxylate (**22**−**24**).* To a solution of **7**, **8** (9 mmol) in anhydrous DMF (17 mL), NaH (0.24 g, 10 mmol) was added at 0 °C, and the reaction mixture was stirred at room temperature for 1.5 h. Then the suitable alkyl or aralkyl halide (13.5 mmol) was added at 0 °C, and the reaction mixture was stirred at room temperature until the reaction was complete (TLC). Then the reaction mixture was poured onto crushed ice. The precipitate was removed by filtration and dried. If there was no precipitate, the solution was extracted with dichloromethane (3 × 50 mL). The organic layer was dried over Na_2SO_4, and the solvent was removed under reduced pressure. The crude product was purified by column chromatography, with dichloromethane as eluting solvent.

*1-(2,5-Dimethoxybenzyl)-4,5,6,7-tetrahydrocyclohepta[b]pyrrol-8(1H)-one (**14**).* This compound was obtained from reaction of **8** with 2,5-dimethoxybenzyl chloride after 2 h. White solid; yield 90%; mp 85.0−85.4 °C; IR (cm^{-1}) 1634 (CO); ^{1}H NMR ($CDCl_3$, 200 MHz) δ 1.79−1.85 (m, 4H, 2 × CH_2), 2.62 (t, 2H, J = 6.1 Hz, CH_2), 2.81 (t, 2H, J = 6.1 Hz, CH_2), 3.67 (s, 3H, CH_3), 3.81 (s, 3H, CH_3), 5.52 (s, 2H, CH_2), 5.99 (d, 1H, J = 2.6 Hz, H-3), 6.35 (d, 1H, J = 2.5 Hz, H-6′), 6.73 (d, 1H, J = 2.6 Hz, H-2), 6.75−6.78 (m, 1H, H-4′), 6.80−6.84 (m, 1H, H-3′); ^{13}C NMR ($CDCl_3$, 50 MHz) δ 21.5, 24.9, 26.4, 41.6, 47.4, 55.5, 55.9, 109.5, 111.0, 112.3, 114.4, 128.5, 128.9, 129.4, 136.5, 150.9, 153.7, 192.7. Anal. Calcd for $C_{18}H_{21}NO_3$: C, 72.22; H, 7.07; N, 4.68. Found: C, 72.07; H, 6.93; N, 4.77.

*1-(3,5-Dimethoxybenzyl)-4,5,6,7-tetrahydrocyclohepta[b]pyrrol-8(1H)-one (**15**).* This compound was obtained from reaction of **8** with 3,5-dimethoxybenzyl chloride after 2 h. Gray solid; yield 90%; mp 60.8−61.7 °C; IR (cm^{-1}) 1625 (CO); ^{1}H NMR ($CDCl_3$, 200 MHz) δ 1.78−1.84 (m, 4H, 2 × CH_2), 2.61 (t, 2H, J = 6.0 Hz, CH_2), 2.81 (t, 2H, J = 6.0 Hz, CH_2), 3.73 (s, 6H, 2 × CH_3), 5.48 (s, 2H, CH_2), 6.01 (d, 1H, J = 2.5 Hz, H-3), 6.22 (d, 2H, J = 2.2 Hz, H-2′ and H-6′), 6.32 (t, 1H, J = 2.2 Hz, H-4′), 6.79 (d, 1H, J = 2.5 Hz, H-2); ^{13}C NMR ($CDCl_3$, 50 MHz) δ 21.5, 24.9, 26.4, 41.6, 52.4, 55.2, 99.0, 104.9, 109.8, 128.8, 129.1, 136.7, 141.1, 160.9, 192.8. Anal. Calcd for $C_{18}H_{21}NO_3$: C, 72.22; H, 7.07; N, 4.68. Found: C, 72.38; H, 7.22; N, 4.54.

*1-(3,4,5-Trimethoxybenzyl)-4,5,6,7-tetrahydrocyclohepta[b]-pyrrol-8(1H)-one (**16**).* This compound was obtained from reaction of **8** with 3,4,5-trimethoxybenzyl chloride after 16 h. White solid; yield 89%; mp 64.6−65.3 °C; IR (cm^{-1}) 1635 (CO); ^{1}H NMR ($CDCl_3$, 200 MHz) δ 1.79−1.85 (m, 4H, 2 × CH_2), 2.63 (t, 2H, J = 6.1 Hz, CH_2), 2.82 (t, 2H, J = 6.1 Hz, CH_2), 3.79 (s, 6H, 2 × CH_3), 3.81 (s, 3H, CH_3), 5.47 (s, 2H, CH_2), 6.03 (d, 1H, J = 2.5 Hz, H-3), 6.33 (s, 2H, H-2′ and H-6′), 6.81 (d, 1H, J = 2.5 Hz, H-2); ^{13}C NMR ($CDCl_3$, 50 MHz) δ 21.5, 25.0, 26.4, 41.6, 52.5, 56.0, 60.8, 104.0, 109.8, 128.9, 129.0, 134.3, 136.9, 137.0, 153.3, 192.9. Anal. Calcd for

https://dx.doi.org/10.1021/acs.jmedchem.0c01315
J. Med. Chem. 2020, 63, 12023−12042

$C_{19}H_{23}NO_4$: C, 69.28; H, 7.04; N, 4.25. Found: C, 69.13; H, 6.86; N, 4.45.

*Ethyl 1-(2,5-Dimethoxybenzyl)-8-oxo-1,4,5,6,7,8-hexahydrocyclohepta[b]pyrrole-2-carboxylate (**22**).* This compound was obtained from reaction of **7** with 2,5-dimethoxybenzyl chloride after 16 h. White solid; yield 81%; mp 92.8−93.4 °C; IR (cm^{-1}) 1711 (CO), 1647 (CO); ^1H NMR (DMSO-d_6, 200 MHz) δ 1.20 (t, 3H, J = 7.1 Hz, CH_3), 1.65−1.81 (m, 4H, 2 × CH_2), 2.59 (t, 2H, J = 5.6 Hz, CH_2), 2.84 (t, 2H, J = 5.6 Hz, CH_2), 3.54 (s, 3H, CH_3), 3.78 (s, 3H, CH_3), 4.16 (q, 2H, J = 7.1 Hz, CH_2), 5.53 (d, 1H, J = 2.9 Hz, H-6′), 5.90 (s, 2H, CH_2), 6.72 (dd, 1H, J = 8.8, 2.9 Hz, H-4′), 6.89 (d, 1H, J = 8.8 Hz, H-3′), 6.90 (s, 1H, H-3); ^{13}C NMR (DMSO-d_6, 50 MHz) δ 13.9, 20.7, 24.4, 24.7, 41.3, 44.8, 55.0, 55.6, 60.3, 110.3, 110.8, 111.6, 117.5, 126.5, 129.1, 133.3, 133.6, 149.9, 153.1, 159.9, 194.0. Anal. Calcd for $C_{21}H_{25}NO_5$: C, 67.91; H, 6.78; N, 3.77. Found: C, 67.84; H, 6.62; N, 3.89.

*Ethyl 1-(3,5-Dimethoxybenzyl)-8-oxo-1,4,5,6,7,8-hexahydrocyclohepta[b]pyrrole-2-carboxylate (**23**).* This compound was obtained from reaction of **7** with 3,5-dimethoxybenzyl chloride after 16 h. White solid; yield 83%; mp 71.8−72.0 °C; IR (cm^{-1}) 1707 (CO), 1647 (CO); ^1H NMR (DMSO-d_6, 200 MHz) δ 1.22 (t, 3H, J = 7.1 Hz, CH_3), 1.72 (m, 4H, 2 × CH_2), 2.61 (t, 2H, J = 6.9 Hz, CH_2), 2.82 (t, 2H, J = 6.9 Hz, CH_2), 3.65 (s, 6H, 2 × CH_3), 4.19 (q, 2H, J = 7.1 Hz, CH_2), 5.94 (s, 4H, CH_2, H-2′ and H-6′), 6.32 (s, 1H, H-4′), 6.88 (s, 1H, H-3); ^{13}C NMR (DMSO-d_6, 50 MHz) δ 14.1, 20.8, 24.4, 24.8, 41.4, 48.2, 55.0, 60.4, 97.8, 103.7, 117.8, 126.3, 133.1, 133.9, 141.9, 160.1, 160.5, 194.3. Anal. Calcd for $C_{21}H_{25}NO_5$: C, 67.91; H, 6.78; N, 3.77. Found: C, 68.07; H, 6.90; N, 3.62.

*Ethyl 1-(3,4,5-Trimethoxybenzyl)-8-oxo-1,4,5,6,7,8-hexahydrocyclohepta[b]pyrrole-2-carboxylate (**24**).* This compound was obtained from reaction of **7** with 3,4,5-trimethoxybenzyl chloride after 24 h. White solid; yield 80%; mp 70.0−70.2 °C; IR (cm^{-1}) 1709 (CO), 1646 (CO); ^1H NMR (DMSO-d_6, 200 MHz) δ 1.24 (t, 3H, J = 7.1 Hz, CH_3), 1.66−1.80 (m, 4H, 2 × CH_2), 2.64 (t, 2H, J = 5.6 Hz, CH_2), 2.82 (t, 2H, J = 5.6 Hz, CH_2), 3.60 (s, 3H, CH_3), 3.64 (s, 6H, 2 × CH_3), 4.22 (q, 2H, J = 7.1 Hz, CH_2), 5.97 (s, 2H, CH_2), 6.16 (s, 2H, H-2′ and H-6′), 6.88 (s, 1H, H-3); ^{13}C NMR (DMSO-d_6, 50 MHz) δ 14.0, 20.8, 24.3, 24.7, 41.4, 48.1, 55.6, 59.9, 60.4, 102.9, 117.8, 126.3, 133.1, 133.9, 135.0, 136.2, 152.8, 160.2, 194.4. Anal. Calcd for $C_{22}H_{27}NO_6$: C, 65.82; H, 6.78; N, 3.49. Found: C, 65.96; H, 6.65; N, 3.35.

*General Procedure for the Preparation of 7-[(Dimethylamino)-methylidene]-1-substituted-4,5,6,7-tetrahydrocyclohepta[b]pyrrol-8(1H)-one (**31**−**33**) and Ethyl 7-[(Dimethylamino)methylidene]-1-substituted-8-oxo-1,4,5,6,7,8-hexahydrocyclohepta[b]pyrrole-2-carboxylate (**39**−**41**). Method A.* To a solution of ketones **22**−**24** (1.3 mmol) in anhydrous DMF (2.5 mL), DMFDMA (0.19 mL, 1.4 mmol) was added, and the reaction mixture was irradiated under MW conditions (power 50 W; pressure (max) 100 psi; temperature (max) 100 °C) until the reaction was complete (TLC).

Method B. To a solution of ketones **22**−**24** (1.3 mmol) in anhydrous DMF (2.5 mL), TBDMAM (0.41 mL, 2 mmol) was added, and the reaction mixture was irradiated under MW conditions (power 50 W; pressure (max) 100 psi; temperature (max) 100 °C) until the reaction was complete (TLC).

Method C. To a solution of ketones **14**−**16** (1.3 mmol) in anhydrous DMF (2.5 mL), DMFDMA (1.73 mL, 13 mmol) was added, and the reaction mixture was irradiated under MW conditions (power 150 W; pressure (max) 150 psi; temperature (max) 130 °C) until the reaction was complete (TLC).

In all cases, the reaction mixtures were poured onto crushed ice. The precipitate was removed by filtration and dried. If there was no precipitate, the solution was extracted with ethyl acetate (3 × 30 mL). The organic layer was dried over Na_2SO_4, and the solvent was removed under reduced pressure.

*7-[(Dimethylamino)methylidene]-1-(2,5-dimethoxybenzyl)-4,5,6,7-tetrahydrocyclohepta[b]pyrrol-8(1H)-one (**31**).* This compound was obtained from reaction of **14** under MW conditions (method C, 40 min). Brown oil; yield 93%; IR (cm^{-1}) 1633 (CO); ^1H NMR ($CDCl_3$, 200 MHz) δ 1.76−1.90 (m, 2H, CH_2), 2.44 (t, 2H, J = 6.7 Hz, CH_2), 2.65 (t, 2H, J = 6.7 Hz, CH_2), 3.06 (s, 6H, 2 × CH_3), 3.64 (s, 3H, CH_3), 3.79 (s, 3H, CH_3), 5.52 (s, 2H, CH_2), 5.94 (d, 1H, J = 2.4 Hz, H-3), 6.31 (d, 1H, J = 2.4 Hz, H-2), 6.65−6.81 (m, 3H, H-3′, H-4′, and H-6′), 7.39 (s, 1H, CH); ^{13}C NMR ($CDCl_3$, 50 MHz) δ 24.2, 24.4, 30.3, 43.2, 46.4, 55.6, 55.8, 107.4, 108.2, 110.9, 112.3, 114.0, 126.7, 129.3, 130.0, 130.5, 148.6, 150.8, 153.7, 188.8. Anal. Calcd for $C_{21}H_{26}N_2O_3$: C, 71.16; H, 7.39; N, 7.90. Found: C, 71.31; H, 7.53; N, 7.77.

*7-[(Dimethylamino)methylidene]-1-(3,5-dimethoxybenzyl)-4,5,6,7-tetrahydrocyclohepta[b]pyrrol-8(1H)-one (**32**).* This compound was obtained from reaction of **15** under MW conditions (method C, 40 min). Brown oil; yield 90%; IR (cm^{-1}) 1635 (CO); ^1H NMR ($CDCl_3$, 200 MHz) δ 1.76−1.90 (m, 2H, CH_2), 2.42 (t, 2H, J = 6.7 Hz, CH_2), 2.65 (t, 2H, J = 6.7 Hz, CH_2), 3.06 (s, 6H, 2 × CH_3), 3.71 (s, 6H, 2 × CH_3), 5.46 (s, 2H, CH_2), 5.95 (d, 1H, J = 2.5 Hz, H-3), 6.22 (d, 2H, J = 2.2 Hz, H-2′ and H-6′), 6.29 (t, 1H, J = 2.2 Hz, H-4′), 6.72 (d, 1H, J = 2.5 Hz, H-2), 7.39 (s, 1H, CH); ^{13}C NMR ($CDCl_3$, 50 MHz) δ 24.1, 24.3, 30.3, 43.2, 51.3, 55.2, 99.1, 104.7, 107.3, 108.3, 126.5, 130.2, 130.5, 141.9, 148.6, 160.8, 188.8. Anal. Calcd for $C_{21}H_{26}N_2O_3$: C, 71.16; H, 7.39; N, 7.90. Found: C, 71.02; H, 7.55; N, 8.11.

*7-[(Dimethylamino)methylidene]-3,4,5-trimethoxybenzyl)-4,5,6,7-tetrahydrocyclohepta[b]pyrrol-8(1H)-one (**33**).* This compound was obtained from reaction of **16** under MW conditions (method C, 120 min). Brown oil; yield 86%; IR (cm^{-1}) 1653 (CO); ^1H NMR ($CDCl_3$, 200 MHz) δ 1.77−1.90 (m, 2H, CH_2), 2.41 (t, 2H, J = 6.6 Hz, CH_2), 2.66 (t, 2H, J = 6.6 Hz, CH_2), 3.08 (s, 6H, 2 × CH_3), 3.77 (s, 6H, 2 × CH_3), 3.79 (s, 3H, CH_3), 5.46 (s, 2H, CH_2), 5.97 (d, 1H, J = 2.5 Hz, H-3), 6.31 (s, 2H, H-2′ and H-6′), 6.74 (d, 1H, J = 2.5 Hz, H-2), 7.41 (s, 1H, CH); ^{13}C NMR ($CDCl_3$, 50 MHz) δ 24.2, 24.3, 30.3, 43.2, 51.4, 55.9, 60.8, 103.7, 107.2, 108.3, 126.4, 130.4, 130.5, 135.2, 136.8, 148.7, 153.2, 188.8. Anal. Calcd for $C_{22}H_{28}N_2O_4$: C, 68.73; H, 7.34; N, 7.29. Found: C, 68.59; H, 7.51; N, 7.08.

*Ethyl 7-[(Dimethylamino)methylidene]-1-(2,5-dimethoxybenzyl)-8-oxo-1,4,5,6,7,8-hexahydrocyclohepta[b]pyrrole-2-carboxylate (**39**).* This compound was obtained from reaction of **22** under MW conditions and used in the next step without purification.

*Ethyl 7-[(Dimethylamino)methylidene]-1-(3,5-dimethoxybenzyl)-8-oxo-1,4,5,6,7,8- hexahydrocyclohepta[b]pyrrole-2-carboxylate (**40**).* This compound was obtained from reaction of **23** under MW conditions (method A, 110 min; method B, 20 min). Pale yellow solid; yield 77% (method A), 94% (method B); mp 139.2−140 °C; IR (cm^{-1}) 1714 (CO), 1698 (CO); ^1H NMR ($CDCl_3$, 200 MHz) δ 1.28 (t, 3H, J = 7.1 Hz, CH_3), 1.73−1.87 (m, 2H, CH_2), 2.39 (t, 2H, J = 6.8 Hz, CH_2), 2.62 (t, 2H, J = 6.8 Hz, CH_2), 3.07 (s, 6H, 2 × CH_3), 3.67 (s, 6H, 2 × CH_3), 4.22 (q, 2H, J = 7.1 Hz, CH_2), 6.06 (s, 2H, CH_2), 6.16 (s, 2H, H-2′ and H-6′), 6.24 (s, 1H, H-4′), 6.77 (s, 1H, H-3), 7.55 (s, 1H, CH); ^{13}C NMR ($CDCl_3$, 50 MHz) δ 14.4, 16.6, 23.7, 30.3, 43.3, 48.6, 55.1, 60.0, 99.0, 104.3, 107.1, 117.0, 125.2, 127.6, 136.6, 142.8, 150.3, 160.9, 161.0, 188.7. Anal. Calcd for $C_{24}H_{30}N_2O_5$: C, 67.59; H, 7.09; N, 6.57. Found: C, 67.71; H, 6.88; N, 6.39.

*Ethyl 7-[(Dimethylamino)methylidene]-8-oxo-1-(3,4,5-trimethoxybenzyl)-1,4,5,6,7,8-hexahydrocyclohepta[b]pyrrole-2-carboxylate (**41**).* This compound was obtained from reaction of **24** under MW conditions (method A, 80 min; method B, 40 min). Brown oil; yield 75% (method A), 99% (method B); IR (cm^{-1}) 1707 (CO), 1635 (CO); ^1H NMR (DMSO-d_6, 200 MHz) δ 1.23 (t, 3H, J = 7.0 Hz, CH_3), 1.70−1.79 (m, 2H, CH_2), 2.30 (t, 2H, J = 6.8 Hz, CH_2), 2.51 (t, 2H, J = 6.8 Hz, CH_2), 2.91 (s, 6H, 2 × CH_3), 3.59 (s, 3H, CH_3), 3.62 (s, 6H, 2 × CH_3), 4.19 (q, 2H, J = 7.0 Hz, CH_2), 5.90 (s, 2H, CH_2), 6.20 (s, 2H, H-2′ and H-6′), 6.77 (s, 1H, H-3), 7.51 (s, 1H, CH); ^{13}C NMR (DMSO-d_6, 50 MHz) δ 14.2, 22.7, 23.1, 29.8, 43.1, 47.2, 55.6, 59.8, 59.9, 103.2, 104.9, 116.8, 123.6, 126.3, 135.5, 136.2, 136.7, 150.6, 152.7, 160.3, 186.5. Anal. Calcd for $C_{25}H_{32}N_2O_6$: C, 65.77; H, 7.07; N, 6.14. Found: C, 65.62; H, 6.89; N, 6.31.

*General Procedure for the Preparation of Ethyl 7-(Hydroxymethylidene)-1-substituted-8-oxo-1,4,5,6,7,8-hexahydrocyclohepta-[b]pyrrole-2-carboxylate (**43**−**50**).* To a suspension of *t*-BuO$^-$K$^+$ (13.5 mmol) in anhydrous toluene (12 mL), at 0 °C and under a N_2 atmosphere, a solution of the appropriate ketone **17**−**24** (4.5 mmol)

https://dx.doi.org/10.1021/acs.jmedchem.0c01315
J. Med. Chem. 2020, 63, 12023−12042

in anhydrous toluene (40 mL) was added, and the reaction mixture was stirred at room temperature for 1.5 h. Then a solution of ethyl formate (1.09 mL, 13.5 mmol) in anhydrous toluene (12 mL) was added at 0 °C, and the reaction mixture was stirred until the reaction was complete (1.5−4 h). The solvent was removed under reduced pressure, and water (50 mL) was added to the residue. The aqueous phase was acidified with 3 N HCl and extracted with dichloromethane (2 × 60 mL). The organic phase was dried over Na_2SO_4, and the solvent was removed under reduced pressure. The crude product was purified by column chromatography with dichloromethane as eluting solvent.

*Ethyl 7-(Hydroxymethylidene)-1-methyl-8-oxo-1,4,5,6,7,8-hexahydrocyclohepta[b]pyrrole-2-carboxylate (**43**).* This compound was obtained from reaction of **17**. Brown oil; yield 80%; IR (cm^{-1}) 3415 (OH), 1704 (CO), 1620 (CO); ^1H NMR ($CDCl_3$, 200 MHz) δ 1.36 (t, 3H, J = 7.1 Hz, CH_3), 1.84−1.97 (m, 2H, CH_2), 2.22 (t, 2H, J = 6.9 Hz, CH_2), 2.69 (t, 2H, J = 6.9 Hz, CH_2), 4.11 (s, 3H, CH_3), 4.31 (q, 2H, J = 7.1 Hz, CH_2), 6.70 (s, 1H, H-3), 7.76 (d, 1H, J = 7.9 Hz, CH), 14.93 (d, 1H, J = 7.9 Hz, OH); ^{13}C NMR ($CDCl_3$, 50 MHz) δ 14.3, 25.0, 25.9, 28.5, 35.0, 60.5, 114.0, 117.0, 127.5, 129.7, 132.8, 160.9, 172.3, 186.3. Anal. Calcd for $C_{14}H_{17}NO_4$: C, 63.87; H, 6.51; N, 5.32. Found: C, 63.99; H, 6.43; N, 5.49.

*Ethyl 7-(Hydroxymethylene)-1-benzyl-8-oxo-1,4,5,6,7,8-hexahydrocyclohepta[b]pyrrole-2-carboxylate (**44**).* This compound was obtained from reaction of **18**. Brown oil; yield 90%; IR (cm^{-1}) 3391 (OH), 1702 (CO), 1619 (CO); ^1H NMR ($CDCl_3$, 200 MHz) δ 1.29 (t, 3H, J = 7.1 Hz, CH_3), 1.84−1.95 (m, 2H, CH_2), 2.13 (t, 2H, J = 6.8 Hz, CH_2), 2.69 (t, 2H, J = 6.8 Hz, CH_2), 4.24 (q, 2H, J = 7.1 Hz, CH_2), 5.99 (s, 2H, CH_2), 6.83 (s, 1H, H-3), 6.92−7.00 (m, 2H, H-2′ and H-6′), 7.16−7.29 (m, 3H, H-3′, H-4′ and H-5′), 7.71 (d, 1H, J = 8.0 Hz, CH), 14.77 (d, 1H, J = 8.0 Hz, OH); ^{13}C NMR ($CDCl_3$, 50 MHz) δ 14.2, 24.5, 25.7, 28.8, 49.2, 60.5, 113.9, 117.9, 126.1, 126.9, 127.0, 128.3, 130.2, 132.7, 139.2, 160.6, 172.5, 186.5. Anal. Calcd for $C_{20}H_{21}NO_4$: C, 70.78; H, 6.24; N, 4.13. Found: C, 70.91; H, 6.09; N, 3.97.

*Ethyl 7-(Hydroxymethylene)-1-(2-methoxybenzyl)-8-oxo-1,4,5,6,7,8-hexahydrocyclohepta[b]pyrrole-2-carboxylate (**45**).* This compound was obtained from reaction of **19**. Brown oil; yield 80%; IR (cm^{-1}) 3400 (OH), 1711 (CO), 1638 (CO); ^1H NMR ($CDCl_3$, 200 MHz) δ 1.26 (t, 3H, J = 7.2 Hz, CH_3), 1.86−1.99 (m, 2H, CH_2), 2.16 (t, 2H, J = 6.4 Hz, CH_2), 2.70 (t, 2H, J = 6.4 Hz, CH_2), 3.82 (s, 3H, CH_3), 4.21 (q, 2H, J = 7.2 Hz, CH_2), 5.94 (s, 2H, CH_2), 6.40 (d, 1H, J = 6.7 Hz, H-3′), 6.77−6.81 (m, 2H, H-5′ and H-6′), 6.83 (s, 1H, H-3), 7.16 (t, 1H, J = 6.7 Hz, H-4′), 7.70 (d, 1H, J = 8.1 Hz, CH), 14.72 (d, 1H, J = 8.1 Hz, OH); ^{13}C NMR ($CDCl_3$, 50 MHz) δ 14.2, 24.5, 25.7, 28.9, 45.6, 55.2, 60.4, 109.8, 113.8, 117.6, 120.3, 125.8, 127.6, 127.8, 128.1, 129.8, 133.2, 156.3, 160.5, 172.3, 186.4. Anal. Calcd for $C_{21}H_{23}NO_5$: C, 68.28; H, 6.28; N, 3.79. Found: C, 68.37; H, 6.16; N, 3.91.

*Ethyl 7-(Hydroxymethylene)-1-(3-methoxybenzyl)-8-oxo-1,4,5,6,7,8-hexahydrocyclohepta[b]pyrrole-2-carboxylate (**46**).* This compound was obtained from reaction of **20**. Colorless oil; yield 68%; IR (cm^{-1}) 3389 (OH), 1707 (CO), 1622 (CO); ^1H NMR ($CDCl_3$, 200 MHz) δ 1.30 (t, 3H, J = 7.1 Hz, CH_3), 1.88−1.98 (m, 2H, CH_2), 2.15 (t, 2H, J = 6.7 Hz, CH_2), 2.69 (t, 2H, J = 6.7 Hz, CH_2), 3.73 (s, 3H, CH_3), 4.24 (q, 2H, J = 7.1 Hz, CH_2), 5.97 (s, 2H, CH_2), 6.52 (d, 1H, J = 2.3 Hz, H-6′), 6.57 (s, 1H, H-2′), 6.72 (dd, 1H, J = 8.2, 2.3 Hz, H-4′), 6.82 (s, 1H, H-3), 7.15 (t, 1H, J = 8.2 Hz, H-5′), 7.72 (s, 1H, CH), 14.76 (s, 1H, OH); ^{13}C NMR ($CDCl_3$, 50 MHz) δ 14.2, 24.6, 25.8, 28.8, 49.1, 55.1, 60.5, 111.8, 112.2, 113.9, 117.9, 118.4, 127.1, 129.4, 130.2, 132.7, 140.9, 159.6, 160.6, 172.5, 186.5. Anal. Calcd for $C_{21}H_{23}NO_5$: C, 68.28; H, 6.28; N, 3.79. Found: C, 68.40; H, 6.46; N, 3.58.

*Ethyl 7-(Hydroxymethylene)-1-(4-methoxybenzyl)-8-oxo-1,4,5,6,7,8-hexahydrocyclohepta[b]pyrrole-2-carboxylate (**47**).* This compound was obtained from reaction of **21**. Pale yellow oil; yield 73%; IR (cm^{-1}) 3399 (OH), 1706 (CO), 1619 (CO); ^1H NMR ($CDCl_3$, 200 MHz) δ 1.31 (t, 3H, J = 7.1 Hz, CH_3), 1.83−1.97 (m, 2H, CH_2), 2.12 (t, 2H, J = 6.6 Hz, CH_2), 2.67 (t, 2H, J = 6.6 Hz, CH_2), 3.75 (s, 3H, CH_3), 4.23 (q, 2H, J = 7.1 Hz, CH_2), 5.91 (s, 2H, CH_2), 6.74 (s, 1H, H-3), 6.76−6.82 (m, 2H, H-3′ and H-5′), 6.91−7.00 (m, 2H, H-2′ and H-6′), 7.73 (d, 1H, J = 7.8 Hz, CH), 14.80 (d, 1H, J = 7.8 Hz, OH); ^{13}C NMR ($CDCl_3$, 50 MHz) δ 14.3, 24.4, 25.7, 28.9, 48.6, 55.2, 60.5, 113.7, 113.9, 117.9, 126.9, 127.7, 130.2, 131.4, 132.6, 158.5, 160.7, 172.5, 186.6. Anal. Calcd for $C_{21}H_{23}NO_5$: C, 68.28; H, 6.28; N, 3.79. Found: C, 68.14; H, 6.41; N, 3.67.

*Ethyl 1-(2,5-Dimethoxybenzyl)-7-(hydroxymethylene)-8-oxo-1,4,5,6,7,8-hexahydrocyclohepta[b]pyrrole-2-carboxylate (**48**).* This compound was obtained from reaction of **22**. Pale yellow oil; yield 76%; IR (cm^{-1}) 3398 (CO), 1709 (CO), 1623 (CO); ^1H NMR ($CDCl_3$, 200 MHz) δ (1.27 (q, 3H, J = 7.1 Hz, CH_2), 1.85−1.99 (m, 2H, CH_2), 2.17 (t, 2H, J = 6.6 Hz, CH_2), 2.70 (t, 2H, J = 6.6 Hz, CH_2), 3.64 (s, 3H, CH_3), 3.78 (s, 3H, CH_3), 4.22 (q, 2H, J = 7.1 Hz, CH_2), 5.92 (s, 2H, CH_2), 6.02 (d, 1H, J = 2.7 Hz, H-6′), 6.63−6.77 (m, 2H, H-3′ and H-4′), 6.83 (s, 1H, H-3), 7.70 (d, 1H, J = 8.2 Hz, CH), 14.73 (d, 1H, J = 8.2 Hz, OH); ^{13}C NMR ($CDCl_3$, 50 MHz) δ 14.2, 24.5, 25.8, 28.8, 45.6, 55.5, 55.8, 60.4, 110.6, 111.1, 113.0, 113.8, 117.7, 127.5, 129.4, 129.8, 133.1, 150.6, 153.5, 160.5, 172.2, 186.4. Anal. Calcd for $C_{22}H_{25}NO_6$: C, 66.15; H, 6.31; N, 3.51. Found: C, 66.29; H, 6.42; N, 3.38.

*Ethyl 1-(3,5-Dimethoxybenzyl)-7-(hydroxymethylene)-8-oxo-1,4,5,6,7,8-hexahydrocyclohepta[b]pyrrole-2-carboxylate (**49**).* This compound was obtained from reaction of **23**. Pale yellow oil; yield 68%; IR (cm^{-1}) 3398 (CO), 1706 (CO), 1609 (CO); ^1H NMR ($CDCl_3$, 200 MHz) δ 1.30 (t, 3H, J = 7.1 Hz, CH_3), 1.85−1.94 (m, 2H, CH_2), 2.15 (t, 2H, J = 6.7 Hz, CH_2), 2.69 (t, 2H, J = 6.7 Hz, CH_2), 3.70 (s, 6H, 2 × CH_3), 4.25 (q, 2H, J = 7.1 Hz, CH_2), 5.95 (s, 2H, CH_2), 6.11 (d, 2H, J = 2.2 Hz, H-2′ and H-6′), 6.28 (t, 1H, J = 2.2 Hz, H-4′), 6.82 (s, 1H, H-3), 7.71 (d, 1H, J = 7.9 Hz, CH), 14.78 (d, 1H, J = 7.9 Hz, OH); ^{13}C NMR ($CDCl_3$, 50 MHz) δ 14.3, 24.5, 25.8, 28.8, 49.1, 55.2, 60.5, 98.8, 104.1, 113.9, 118.0, 127.1, 130.2, 132.7, 141.8, 160.6, 160.8, 172.4, 186.6. Anal. Calcd for $C_{22}H_{25}NO_6$: C, 66.15; H, 6.31; N, 3.51. Found: C, 65.93; H, 6.15; N, 3.77.

*Ethyl 7-(Hydroxymethylene)-8-oxo-1-(3,4,5-trimethoxybenzyl)-1,4,5,6,7,8-hexahydrocyclohepta[b]pyrrole-2-carboxylate (**50**).* This compound was obtained from reaction of **24**. Yellow oil; yield 60%; IR (cm^{-1}) 3410 (OH), 1710 (CO), 1647 (CO); ^1H NMR ($CDCl_3$, 200 MHz) δ 1.33 (t, 3H, J = 7.1 Hz, CH_3), 1.88−1.98 (m, 2H, CH_2), 2.13 (t, 2H, J = 6.8 Hz, CH_2), 2.68 (t, 2H, J = 6.8 Hz, CH_2), 3.74 (s, 6H, 2 × CH_3), 3.78 (s, 3H, CH_3), 4.28 (q, 2H, J = 7.1 Hz, CH_2), 5.94 (s, 2H, CH_2), 6.28 (s, 2H, H-2′ and H-6′), 6.81 (s, 1H, H-3), 7.74 (d, 1H, J = 8.0 Hz, CH), 14.83 (d, 1H, J = 8.0 Hz, OH); ^{13}C NMR ($CDCl_3$, 50 MHz) δ 14.3, 24.4, 25.7, 28.9, 48.9, 55.9, 60.6, 60.8, 100.0, 103.7, 114.0, 118.0, 126.7, 130.3, 134.9, 136.9, 153.1, 160.8, 172.5, 186.9. Anal. Calcd for $C_{23}H_{27}NO_7$: C, 64.32; H, 6.34; N, 3.26. Found: C, 64.21; H, 6.48; N, 3.09.

*General Procedure for the Preparation of Pyrrolo[2′,3′:3,4]-cyclohepta[1,2-d][1,2]oxazole (**51**−**68**).* To a solution of the suitable enaminoketones **25**−**42** or hydroxymethylene ketones **43**−**50** (1.5 mmol) in ethanol (6 mL) and acetic acid (3 mL), hydroxylamine hydrochloride (1.65 mmol) was added, and the reaction mixture was heated at reflux for 1 h. Then the reaction mixture was poured onto crushed ice. The precipitate was removed by filtration and dried. If there was no precipitate, the solution was extracted with dichloromethane (3 × 20 mL). The organic layer was dried over Na_2SO_4, and the solvent was removed under reduced pressure. The crude product was purified by column chromatography with dichloromethane/ethyl acetate 95:5 as eluting solvent.

*9-(Phenylsulfonyl)-4,5,6,9-tetrahydropyrrolo[2′,3′:3,4]-cyclohepta[1,2-d][1,2]oxazole (**51**).* This compound was obtained from reaction of **25**. Orange solid; yield 60%; mp 140.3−141.0 °C; ^1H NMR ($CDCl_3$, 200 MHz) δ 1.88−1.98 (m, 2H, CH_2), 2.65−2.77 (m, 4H, 2 × CH_2), 6.20 (d, 1H, J = 3.3 Hz, H-7), 7.49−7.62 (m, 4H, H-8, H-3′, H-4′, and H-5′), 7.96 (s, 1H, H-3), 8.06 (d, 2H, J = 7.9 Hz, H-2′ and H-6′); ^{13}C NMR ($CDCl_3$, 50 MHz) δ 23.5, 23.7, 28.0, 113.1, 113.9, 118.9, 125.6, 128.1, 128.9, 133.1, 133.8, 138.9, 151.5, 156.1. Anal. Calcd for $C_{16}H_{14}N_2O_3S$: C, 61.13; H, 4.49; N, 8.91. Found: C, 61.31; H, 4.40; N, 9.10.

*9-Methyl-4,5,6,9-tetrahydropyrrolo[2′,3′:3,4]cyclohepta[1,2-d]-[1,2]oxazole (**52**).* This compound was obtained from reaction of **26**.

https://dx.doi.org/10.1021/acs.jmedchem.0c01315
J. Med. Chem. 2020, 63, 12023−12042

White solid; yield 75%; mp 60.4 °C; ^{1}H NMR ($CDCl_3$, 200 MHz) δ 1.89−2.00 (m, 2H, CH_2), 2.74 (t, 2H, J = 6.0 Hz, CH_2), 2.87 (t, 2H, J = 6.0 Hz, CH_2), 3.95 (s, 3H, CH_3), 5.95 (d, 1H, J = 2.5 Hz, H-7), 6.58 (d, 1H, J = 2.5 Hz, H-8), 8.01 (s, 1H, H-3); ^{13}C NMR ($CDCl_3$, 50 MHz) δ 23.2, 24.4, 28.8, 37.6, 99.9, 109.3, 111.1, 125.5, 127.3, 151.4, 159.7. Anal. Calcd for $C_{11}H_{12}N_2O$: C, 70.19; H, 6.43; N, 14.88. Found: C, 70.39; H, 6.23; N, 14.63.

*9-Benzyl-4,5,6,9-tetrahydropyrrolo[2′,3′:3,4]cyclohepta[1,2-d]-[1,2]oxazole (**53**).* This compound was obtained from reaction of **27**. Pale yellow solid; yield 83%; mp 61.3 °C; ^{1}H NMR ($CDCl_3$, 200 MHz) δ 1.88−2.00 (m, 2H, CH_2), 2.72 (t, 2H, J = 6.2 Hz, CH_2), 2.88 (t, 2H, J = 6.2 Hz, CH_2), 5.52 (s, 2H, CH_2), 6.02 (d, 1H, J = 2.6 Hz, H-7), 6.67 (d, 1H, J = 2.6 Hz, H-8), 7.12−7.33 (m, 5H, Ar), 7.94 (s, 1H, H-3); ^{13}C NMR ($CDCl_3$, 50 MHz) δ 23.1, 24.3, 28.8, 53.0, 110.2, 111.4, 119.1, 125.2, 126.9, 127.3, 127.7, 128.5, 138.3, 151.4, 159.3. Anal. Calcd for $C_{17}H_{16}N_2O$: C, 77.25; H, 6.10; N, 10.60. Found: C, 77.60; H, 5.75; N, 10.25.

*9-(2-Methoxybenzyl)-4,5,6,9-tetrahydropyrrolo[2′,3′:3,4]-cyclohepta[1,2-d][1,2]oxazole (**54**).* This compound was obtained from reaction of **28**. Pale yellow solid; yield 70%; mp 80.4 °C; ^{1}H NMR ($CDCl_3$, 200 MHz) δ 1.91−2.02 (m, 2H, CH_2), 2.74 (t, 2H, J = 5.5 Hz, CH_2), 2.90 (t, 2H, J = 5.5 Hz, CH_2), 3.87 (s, 3H, CH_3), 5.54 (s, 2H, CH_2), 6.01 (d, 1H, J = 2.6 Hz, H-7) 6.65 (d, 1H, J = 2.6 Hz, H-8), 6.71−6.89 (m, 3H, Ar), 7.15−7.23 (m, 1H, Ar), 7.95 (s, 1H, H-3); ^{13}C NMR ($CDCl_3$, 50 MHz) δ 23.2, 24.4, 28.8, 48.2, 55.3, 109.9, 110.0, 111.2, 119.2, 120.6, 125.3, 127.0, 127.3, 127.5, 128.4, 151.3, 156.5, 159.5. Anal. Calcd for $C_{18}H_{18}N_2O_2$: C, 73.45; H, 6.16; N, 9.52. Found: C, 73.63; H, 5.85; N, 9.60.

*9-(3-Methoxybenzyl)-4,5,6,9-tetrahydropyrrolo[2′,3′:3,4]-cyclohepta[1,2-d][1,2]oxazole (**55**).* This compound was obtained from reaction of **29**. Yellow solid; yield 83%; mp 67.6 °C; ^{1}H NMR ($CDCl_3$, 200 MHz) δ 1.89−2.00 (m, 2H, CH_2), 2.73 (t, 2H, J = 5.5 Hz, CH_2), 2.88 (t, 2H, J = 5.5 Hz, CH_2), 3.74 (s, 3H, CH_3), 5.50 (s, 2H, CH_2), 6.02 (d, 1H, J = 2.6 Hz, H-7) 6.68 (d, 1H, J = 2.6 Hz, H-8), 6.71−6.78 (m, 3H, H-2′, H-4′ and H-6′), 7.20 (t, 1H, J = 7.9 Hz, H-5′), 7.95 (s, 1H, H-3); ^{13}C NMR ($CDCl_3$, 50 MHz) δ 23.2, 24.4, 28.8, 52.9, 55.1, 110.2, 111.4, 112.5, 112.7, 119.1, 119.2, 125.2, 127.7, 129.6, 140.0, 151.4, 159.3, 159.7. Anal. Calcd for $C_{18}H_{18}N_2O_2$: C, 73.45; H, 6.16; N, 9.52. Found: C, 73.31; H, 6.24; N, 9.50.

*9-(4-Methoxybenzyl)-4,5,6,9-tetrahydropyrrolo[2′,3′:3,4]-cyclohepta[1,2-d][1,2]oxazole (**56**).* This compound was obtained from reaction of **30**. Yellow solid; yield 68%; mp 101 °C; ^{1}H NMR ($CDCl_3$, 200 MHz) δ 1.88−1.99 (m, 2H, CH_2), 2.73 (t, 2H, J = 5.8 Hz, CH_2), 2.88 (t, 2H, J = 5.8 Hz, CH_2), 3.76 (s, 3H, CH_3), 5.45 (s, 2H, CH_2), 6.01 (d, 1H, J = 2.5 Hz, H-7) 6.68 (d, 1H, J = 2.5 Hz, H-8), 6.82 (d, 2H, J = 8.5 Hz, H-3′ and H-5′), 7.12 (d, 2H, J = 8.5 Hz, H-2′ and H-6′), 7.95 (s, 1H, H-3); ^{13}C NMR ($CDCl_3$, 50 MHz) δ 23.2, 24.4, 28.8, 52.5, 55.2, 110.0, 111.5, 113.9, 118.9, 124.9, 127.7, 128.5, 130.2, 151.9, 158.8, 156.9. Anal. Calcd for $C_{18}H_{18}N_2O_2$: C, 73.45; H, 6.16; N, 9.52. Found: C, 73.55; H, 6.04; N, 9.44.

*9-(2,5-Dimethoxybenzyl)-4,5,6,9-tetrahydropyrrolo[2′,3′:3,4]-cyclohepta[1,2-d][1,2]oxazole (**57**).* This compound was obtained from reaction of **31**. White solid; yield 78%; mp 116.6 °C; ^{1}H NMR ($CDCl_3$, 200 MHz) δ 1.90−2.01 (m, 2H, CH_2), 2.74 (t, 2H, J = 6.2 Hz, CH_2), 2.89 (t, 2H, J = 6.2 Hz, CH_2), 3.63 (s, 3H, CH_3), 3.83 (s, 3H, CH_3), 5.51 (s, 2H, CH_2), 6.00 (d, 1H, J = 2.6 Hz, H-7), 6.29 (d, 1H, J = 2.6 Hz, H-8), 6.67−6.82 (m, 3H, H-3′, H-4′ and H-6′), 7.95 (s, 1H, H-3); ^{13}C NMR ($CDCl_3$, 50 MHz) δ 23.2, 24.4, 28.8, 48.2, 55.5, 55.9, 110.6, 110.9, 111.2, 112.1, 114.0, 119.2, 125.4, 127.4, 128.2, 150.8, 151.3, 153.6, 159.4. Anal. Calcd for $C_{19}H_{20}N_2O_3$: C, 70.35; H, 6.21; N, 8.64. Found: C, 70.49; H, 6.38; N, 8.47.

*9-(3,5-Dimethoxybenzyl)-4,5,6,9-tetrahydropyrrolo[2′,3′:3,4]-cyclohepta[1,2-d][1,2]oxazole (**58**).* This compound was obtained from reaction of **32**. Yellow solid; yield 76%; mp 118.6 °C; ^{1}H NMR ($CDCl_3$, 200 MHz) δ 1.89−2.00 (m, 2H, CH_2), 2.73 (t, 2H, J = 6.0 Hz, CH_2), 2.88 (t, 2H, J = 6.0 Hz, CH_2), 3.72 (s, 6H, 2 × CH_3), 5.46 (s, 2H, CH_2), 6.01 (d, 1H, J = 2.6 Hz, H-7), 6.27 (d, 2H, J = 2.2 Hz, H-2′ and H-6′), 6.32 (t, 1H, J = 2.2 Hz, H-4′), 6.67 (d, 1H, J = 2.6 Hz, H-8), 7.95 (s, 1H, H-3); ^{13}C NMR ($CDCl_3$, 50 MHz) δ 23.2, 24.3, 28.8, 53.0, 55.2, 99.1, 104.8, 110.2, 111.4, 119.1, 125.2, 127.7, 140. 8, 151.4, 159.3, 160.9. Anal. Calcd for $C_{19}H_{20}N_2O_3$: C, 70.35; H, 6.21; N, 8.64. Found: C, 70.55; H, 6.36; N, 8.49.

*9-(3,4,5-Trimethoxybenzyl)-4,5,6,9-tetrahydropyrrolo[2′,3′:3,4]-cyclohepta[1,2-d][1,2]oxazole (**59**).* This compound was obtained from reaction of **33**. White solid; yield 74%; mp 104.5 °C; ^{1}H NMR ($CDCl_3$, 200 MHz) δ 1.89−2.00 (m, 2H, CH_2), 2.74 (t, 2H, J = 6.0 Hz, CH_2), 2.88 (t, 2H, J = 6.0 Hz, CH_2), 3.77 (s, 6H, 2 × CH_3), 3.80 (s, 3H, CH_3), 5.45 (s, 2H, CH_2), 6.02 (d, 1H, J = 2.6 Hz, H-7), 6.39 (s, 2H, H-2′ and H-6′), 6.69 (d, 1H, J = 2.6 Hz, H-8), 7.97 (s, 1H, H-3); ^{13}C NMR ($CDCl_3$, 50 MHz) δ 23.3, 24.4, 28.8, 53.2, 56.0, 60.8, 104.1, 110.2, 111.5, 119.1, 125.1, 127.9, 133.8, 137.1, 151.5, 153.3, 159.3. Anal. Calcd for $C_{20}H_{22}N_2O_4$: C, 67.78; H, 6.26; N, 7.90. Found: C, 67.87; H, 6.17; N, 7.81.

*Ethyl 9-Methyl-4,5,6,9-tetrahydropyrrolo[2′,3′:3,4]cyclohepta-[1,2-d][1,2]oxazole-8-carboxylate (**60**).* This compound was obtained from reaction of **34** (yield 90%) or **43** (yield 86%). White solid; mp 91.7 °C; IR (cm^{-1}) 1699 (CO); ^{1}H NMR ($CDCl_3$, 200 MHz) δ 1.36 (t, 3H, J = 7.1 Hz, CH_3), 1.89−2.00 (m, 2H, CH_2), 2.74−2.85 (m, 4H, 2 × CH_2), 4.24−4.35 (m, 5H, CH_2 and CH_3), 6.76 (s, 1H, H-7), 8.08 (s, 1H, H-3); ^{13}C NMR ($CDCl_3$, 50 MHz) δ 14.4, 23.4, 24.5, 28.1, 35.2, 60.1, 114.8, 114.9, 118.0, 124.2, 126.1, 151.8, 158.3, 161.1. Anal. Calcd for $C_{14}H_{16}N_2O_3$: C, 64.60; H, 6.20; N, 10.76. Found: C, 64.45; H, 5.96; N, 11.00.

*Ethyl 9-Benzyl-4,5,6,9-tetrahydropyrrolo[2′,3′:3,4]cyclohepta-[1,2-d][1,2]oxazole-8-carboxylate (**61**).* This compound was obtained from reaction of **35** (yield 70%) or **44** (yield 68%). Gray solid; mp 149.4 °C; IR (cm^{-1}) 1695 (CO); ^{1}H NMR ($CDCl_3$, 200 MHz) δ 1.30 (t, 3H, J = 7.1 Hz, CH_3), 1.92−2.00 (m, 2H, CH_2), 2.71−2.89 (m, 4H, 2 × CH_2), 4.24 (q, 2H, J = 7.1 Hz, CH_2), 6.17 (s, 2H, CH_2), 6.87 (s, 1H, H-7), 6.99−7.07 (m, 2H, H-2′ and H-6′), 7.13−7.30 (m, 3H, H-3′, H-4′ and H-5′), 8.00 (s, 1H, H-3); ^{13}C NMR ($CDCl_3$, 50 MHz) δ 14.3, 23.4, 24.5, 28.2, 50.1, 60.2, 115.1, 119.0, 124.2, 125.5, 126.1, 126.7, 126.8, 128.3, 139.0, 151.7, 157.8, 160.8. Anal. Calcd for $C_{20}H_{20}N_2O_3$: C, 71.41; H, 5.99; N, 8.33. Found: C, 71.26; H, 6.14; N, 8.31.

*Ethyl 9-(2-Methoxybenzyl)-4,5,6,9-tetrahydropyrrolo[2′,3′:3,4]-cyclohepta[1,2-d][1,2]oxazole-8-carboxylate (**62**).* This compound was obtained from reaction of **36** (yield: 74%) or **45** (yield: 70%). White solid; mp 137.5−138.3 °C; IR (cm^{-1}) 1700 (CO); ^{1}H NMR ($CDCl_3$, 200 MHz) δ 1.26 (t, 3H, J = 7.1 Hz, CH_3), 1.89−2.06 (m, 2H, CH_2), 2.77 (t, 2H, J = 6.1 Hz, CH_2), 2.86 (t, 2H, J = 6.1 Hz, CH_2), 3.89 (s, 3H, CH_3), 4.20 (q, 2H, J = 7.1 Hz, CH_2), 6.11 (s, 2H, CH_2), 6.29 (d, 1H, J = 7.5 Hz, H-3′), 6.68−6.88 (m, 3H, H-7, H-5′ and H-6′), 7.13 (t, 1H, J = 8.1 Hz, H-4′), 7.97 (s, 1H, H-3); ^{13}C NMR ($CDCl_3$, 50 MHz) δ 14.2, 23.5, 24.5, 28.2, 46.5, 55.3, 60.1, 109.8, 114.9, 118.8, 120.3, 124.7, 125.0, 125.8, 126.5, 127.5, 128.0, 151.6, 156.2, 158.0, 160.6. Anal. Calcd for $C_{21}H_{22}N_2O_4$: C, 68.84; H, 6.05; N, 7.65. Found: C, 68.96; H, 5.78; N, 7.53.

*Ethyl 9-(3-Methoxybenzyl)-4,5,6,9-tetrahydropyrrolo[2′,3′:3,4]-cyclohepta[1,2-d][1,2]oxazole-8-carboxylate (**63**).* This compound was obtained from reaction of **37** (yield 82%) or **46** (yield 80%). Pale yellow solid; mp 98−98.4 °C; IR (cm^{-1}) 1696 (CO); ^{1}H NMR ($CDCl_3$, 200 MHz) δ 1.30 (t, 3H, J = 7.1 Hz, CH_3), 1.91−2.00 (m, 2H, CH_2), 2.72−2.87 (m, 4H, 2 × CH_2), 3.71 (s, 3H, CH_3), 4.24 (q, 2H, J = 7.1 Hz, CH_2), 6.15 (s, 2H, CH_2), 6.54−6.73 (m, 3H, H-2′, H-4′ and H-6′), 6.86 (s, 1H, H-7), 7.14 (t, 1H, J = 7.9 Hz, H-5′), 8.00 (s, 1H, H-3); ^{13}C NMR ($CDCl_3$, 50 MHz) δ 14.3, 23.4, 24.5, 28.2, 49.9, 55.0, 60.2, 111.8, 112.0, 115.0, 118.4, 119.0, 124.3, 125.5, 126.7, 129.3, 140.7, 151.7, 157.8, 159.6, 160.8. Anal. Calcd for $C_{21}H_{22}N_2O_4$: C, 68.84; H, 6.05; N, 7.65. Found: C, 68.53; H, 6.36; N, 7.41.

*Ethyl 9-(4-Methoxybenzyl)-4,5,6,9-tetrahydropyrrolo[2′,3′:3,4]-cyclohepta[1,2-d][1,2]oxazole-8-carboxylate (**64**).* This compound was obtained from reaction of **38** (yield 84%) or **47** (yield 82%). White solid; mp 93.9 °C; IR (cm^{-1}) 1690 (CO); ^{1}H NMR ($CDCl_3$, 200 MHz) δ 1.32 (t, 3H, J = 7.1 Hz, CH_3), 1.88−1.99 (m, 2H, CH_2), 2.72−2.86 (m, 4H, 2 × CH_2), 3.74 (s, 3H, CH_3), 4.26 (q, 2H, J = 7.1 Hz, CH_2), 6.09 (s, 2H, CH_2), 6.76 (d, 2H, J = 6.8 Hz, H-3′ and H-5′), 6.85 (s, 1H, H-7), 7.01 (d, 2H, J = 8.6 Hz, H-2′ and H-6′), 8.02 (s, 1H, H-3); ^{13}C NMR ($CDCl_3$, 50 MHz) δ 14.3, 23.4, 24.5, 28.2, 49.4, 55.1, 60.2, 113.7, 115.0, 119.0, 124.3, 125.5, 126.7, 127.6, 131.1,

https://dx.doi.org/10.1021/acs.jmedchem.0c01315
J. Med. Chem. 2020, 63, 12023−12042

151.8, 157.8, 158.4, 160.9. Anal. Calcd for $C_{21}H_{22}N_2O_4$: C, 68.84; H, 6.05; N, 7.65. Found: C, 68.61; H, 6.20; N, 7.87.

*Ethyl 9-(2,5-Dimethoxybenzyl)-4,5,6,9-tetrahydropyrrolo-[2′,3′:3,4]cyclohepta[1,2-d][1,2]oxazole-8-carboxylate (**65**).* This compound was obtained from reaction of **39** (yield 74%) or **48** (yield 72%). White solid; mp 94.9 °C; IR (cm^{-1}) 1690 (CO); ^1H NMR ($CDCl_3$, 200 MHz) δ 1.26 (t, 3H, J = 7.1 Hz, CH_3), 1.93−2.02 (m, 2H, CH_2), 2.74−2.88 (m, 4H, 2 × CH_2), 3.60 (s, 3H, CH_3), 3.85 (s, 3H, CH_3), 4.20 (q, 2H, J = 7.1 Hz, CH_2), 5.91 (d, 1H, J = 2.6 Hz, H-6′), 6.08 (s, 2H, CH_2), 6.63 (dd, 1H, J = 8.7, 2.6 Hz, H-4′), 6.76 (d, 1H, J = 8.7 Hz, H-3′), 6.87 (s, 1H, H-7), 7.97 (s, 1H, H-3); ^{13}C NMR ($CDCl_3$, 50 MHz) δ 14.2, 23.5, 24.5, 28.2, 46.5, 55.4, 55.9, 60.1, 110.4, 110.6, 112.6, 114.9, 118.9, 124.5, 125.6, 126.5, 129.5, 150.6, 151.6, 153.5, 157.9, 160.6. Anal. Calcd for $C_{22}H_{24}N_2O_5$: C, 66.65; H, 6.10; N, 7.07. Found: C, 66.49; H, 6.36; N, 6.81.

*Ethyl 9-(3,5-Dimethoxybenzyl)-4,5,6,9-tetrahydropyrrolo-[2′,3′:3,4]cyclohepta[1,2-d][1,2]oxazole-8-carboxylate (**66**).* This compound was obtained from reaction of **40** (yield 82%) or **49** (yield 80%). White solid; mp 114 °C; IR (cm^{-1}) 1701 (CO); ^1H NMR ($CDCl_3$, 200 MHz) δ 1.31 (t, 3H, J = 7.1 Hz, CH_3), 1.92−2.00 (m, 2H, CH_2), 2.64−2.86 (m, 4H, 2 × CH_2), 3.70 (s, 6H, 2 × CH_3), 4.24 (q, 2H, J = 7.1 Hz, CH_2), 6.07−6.28 (m, 4H, CH_2, H-2′ and H-6′), 6.26 (s, 1H, H-4′), 6.86 (s, 1H, H-7), 8.00 (s, 1H, H-3); ^{13}C NMR ($CDCl_3$, 50 MHz) δ 14.3, 23.4, 24.5, 28.2, 50.0, 55.2, 60.2, 98.6, 100.0, 104.1, 115.1, 119.1, 124.2, 126.7, 141.6, 151.7, 157.8, 160.7, 160.8. Anal. Calcd for $C_{22}H_{24}N_2O_5$: C, 66.65; H, 6.10; N, 7.07. Found: C, 66.84; H, 6.42; N, 6.75.

*Ethyl 9-(3,4,5-Trimethoxybenzyl)-4,5,6,9-tetrahydropyrrolo-[2′,3′:3,4]cyclohepta[1,2-d][1,2]oxazole-8-carboxylate (**67**).* This compound was obtained from reaction of **41** (yield 76%) or **50** (yield 75%). Pale yellow solid; mp 112.9−113.1 °C; IR (cm^{-1}) 1696 (CO); ^1H NMR ($CDCl_3$, 200 MHz) δ 1.33 (t, 3H, J = 7.1 Hz, CH_3), 1.88−1.99 (m, 2H, CH_2), 2.73−2.87 (m, 4H, 2 × CH_2), 3.72 (s, 6H, 2 × CH_3), 3.77 (s, 3H, CH_3), 4.28 (q, 2H, J = 7.1 Hz, CH_2), 6.11 (s, 2H, CH_2), 6.29 (s, 2H, H-2′ and H-6′), 6.86 (s, 1H, H-7), 8.04 (s, 1H, H-3); ^{13}C NMR ($CDCl_3$, 50 MHz) δ 14.4, 23.6, 24.5, 28.1, 49.8, 55.9, 60.3, 60.8, 100.0, 103.5, 115.1, 119.1, 124.2, 125.5, 126.9, 134.6, 151.8, 153.1, 157.8, 161.0. Anal. Calcd for $C_{23}H_{26}N_2O_6$: C, 64.78; H, 6.15; N, 6.57. Found: C, 64.44; H, 6.05; N, 6.67.

*Methyl 9-Benzyl-4,5,6,9-tetrahydropyrrolo[2′,3′:3,4]cyclohepta-[1,2-d][1,2]oxazole-8-carboxylate (**68**).* This compound was obtained from reaction of **42**. White solid; yield 78%; mp 150.3 °C; IR (cm^{-1}) 1698 (CO); ^1H NMR ($CDCl_3$, 200 MHz) δ 1.89−2.00 (m, 2H, CH_2), 2.77 (t, 2H, J = 6.2 Hz, CH_2), 2.84 (t, 2H, J = 6.2 Hz, CH_2), 3.78 (s, 3H, CH_3), 6.17 (s, 2H, CH_2), 6.86 (s, 1H, H-7), 6.98 (s, 2H, J = 9.7 Hz, H-2′ and H-6′), 7.12−7.28 (m, 3H, H-3′, H-4′ and H-5′), 8.01 (s, 1H, H-3); ^{13}C NMR ($CDCl_3$, 200 MHz) δ 23.3, 24.5, 28.1, 50.0, 51.3, 115.1, 119.1, 123.8, 125.6, 126.0, 126.7, 126.8, 128.3, 138.9, 151.7, 157.7, 161.2. Anal. Calcd for $C_{19}H_{18}N_2O_3$: C, 70.79; H, 5.63; N, 8.69. Found: C, 70.65; H, 5.77; N, 8.58.

*General Procedure for the Preparation of Chloropyrrolo-[2′,3′:3,4]cyclohepta[1,2-d][1,2]oxazole (**69**−**76**).* To a solution of **60**−**66**, **52** (1 mmol) in anhydrous DMF (5 mL) a solution of *N*-chlorosuccinimide (1.5 mmol) in anhydrous DMF (2 mL) was added, and the reaction mixture was stirred for 16 h at room temperature. Then, the reaction mixture was poured onto crushed ice. The precipitate was removed by filtration and dried. In the absence of a precipitate, the solution was extracted with dichloromethane (3 × 30 mL). The organic layer was dried over Na_2SO_4, and the solvent was removed under reduced pressure. The crude product was purified by column chromatography with dichloromethane/ethyl acetate 98:2 as eluting solvent.

*Ethyl 7-Chloro-9-methyl-4,5,6,9-tetrahydropyrrolo[2′,3′:3,4]-cyclohepta[1,2-d][1,2]oxazole-8-carboxylate (**69**).* This compound was obtained from reaction of **60**. White solid; yield 60%; mp 88.2 °C; IR (cm^{-1}) 1695 (CO); ^1H NMR ($CDCl_3$, 200 MHz) δ 1.43 (t, 3H, J = 7.1 Hz, CH_3), 1.94−2.04 (m, 2H, CH_2), 2.77−2.89 (m, 4H, 2 × CH_2), 4.29 (s, 3H, CH_3), 4.40 (q, 2H, J = 7.1 Hz, CH_2), 8.08 (s, 1H, H-3); ^{13}C NMR ($CDCl_3$, 50 MHz) δ 14.4, 23.3, 24.6, 25.4, 36.2, 60.7, 115.7, 119.5, 121.4, 124.1, 124.5, 151.7, 157.7, 160.6. Anal. Calcd for $C_{14}H_{15}ClN_2O_3$: C, 57.05; H, 5.13; N, 9.50. Found: C, 57.16; H, 5.00; N, 9.57.

*Ethyl 7-Chloro-9-benzyl-4,5,6,9-tetrahydropyrrolo[2′,3′:3,4]-cyclohepta[1,2-d][1,2]oxazole-8-carboxylate (**70**).* This compound was obtained from reaction of **61**. White solid; yield 75%; mp 141.8−142.4 °C; IR (cm^{-1}) 1696 (CO); ^1H NMR ($CDCl_3$, 200 MHz) δ 1.32 (t, 3H, J = 7.1 Hz, CH_3), 1.90−2.02 (m, 2H, CH_2), 2.73−2.89 (m, 4H, 2 × CH_2), 4.30 (q, 2H, J = 7.1 Hz, CH_2), 6.12 (s, 2H, CH_2), 6.99 (d, 2H, J = 7.2 Hz, H-2′ and H-6′), 7.14−7.26 (m, 3H, H-3′, H-4′ and H-5′), 8.02 (s, 1H, H-3); ^{13}C NMR ($CDCl_3$, 50 MHz) δ 14.2, 23.1, 24.4, 25.3, 50.8, 60.8, 116.1, 120.4, 121.2, 124.1, 124.8, 126.0, 127.0, 128.4, 138.5, 151.7, 157.0, 160.3. Anal. Calcd for $C_{20}H_{19}ClN_2O_3$: C, 64.78; H, 5.16; N, 7.55. Found: C, 64.98; H, 5.06; N, 7.65.

*Ethyl 7-Chloro-9-(2-methoxybenzyl)-4,5,6,9-tetrahydropyrrolo-[2′,3′:3,4]cyclohepta[1,2-d][1,2]oxazole-8-carboxylate (**71**).* This compound was obtained from reaction of **62**. Yellow solid; yield 74%; mp 159.8 °C; IR (cm^{-1}) 1696 (CO); ^1H NMR ($CDCl_3$, 200 MHz) δ 1.26 (t, 3H, J = 7.1 Hz, CH_3), 1.92−2.03 (m, 2H, CH_2), 2.77 (t, 2H, J = 5.8 Hz, CH_2), 2.87 (t, 2H, J = 5.8 Hz, CH_2), 3.85 (s, 3H, CH_3), 4.26 (q, 2H, J = 7.1 Hz, CH_2), 6.05 (s, 2H, CH_2), 6.41 (d, 1H, J = 7.4 Hz, H-3′), 6.71−6.85 (m, 2H, H-5′ and H-6′), 7.14 (t, 1H, J = 7.4 Hz, H-4′), 8.00 (s, 1H, H-3); ^{13}C NMR ($CDCl_3$, 50 MHz) δ 14.0, 23.2, 24.4, 25.3, 42.3, 55.3, 60.7, 109.8, 115.8, 120.0, 120.4, 121.5, 124.3, 124.5, 125.4, 127.4, 127.8, 151.6, 156.2, 157.2, 160.1. Anal. Calcd for $C_{21}H_{21}ClN_2O_4$: C, 62.92; H, 5.28; N, 6.99. Found: C, 62.72; H, 5.51; N, 6.91.

*Ethyl 7-Chloro-9-(3-methoxybenzyl)-4,5,6,9-tetrahydropyrrolo-[2′,3′:3,4]cyclohepta[1,2-d][1,2]oxazole-8-carboxylate (**72**).* This compound was obtained from reaction of **63**. Green solid; yield 65%; mp 92.8−93.5 °C; IR (cm^{-1}) 1695 (CO); ^1H NMR ($CDCl_3$, 200 MHz) δ 1.33 (t, 3H, J = 7.1 Hz, CH_3), 1.90−2.02 (m, 2H, CH_2), 2.73−2.89 (m, 4H, 2 × CH_2), 3.72 (s, 3H, CH_3), 4.30 (q, 2H, J = 7.1 Hz, CH_2), 6.10 (s, 2H, CH_2), 6.53−6.61 (m, 2H, H-2′ and H-6′), 6.70 (dd, 1H, J = 7.9, 2.3 Hz, H-4′), 7.15 (t, 1H, J = 7.9 Hz, H-5′), 8.03 (s, 1H, H-3); ^{13}C NMR ($CDCl_3$, 50 MHz) δ 14.2, 23.1, 24.4, 25.3, 50.6, 55.1, 60.8, 111.9, 112.1, 116.1, 118.3, 120.4, 121.1, 124.7, 129.4, 138.4, 140.2, 151.7, 157.0, 159.6, 160.3. Anal. Calcd for $C_{21}H_{21}ClN_2O_4$: C, 62.92; H, 5.28; N, 6.99. Found: C, 62.84; H, 5.17; N, 7.08.

*Ethyl 7-Chloro-9-(4-methoxybenzyl)-4,5,6,9-tetrahydropyrrolo-[2′,3′:3,4]cyclohepta[1,2-d][1,2]oxazole-8-carboxylate (**73**).* This compound was obtained from reaction of **64**. White solid; yield 70%; mp 118.1 °C; IR (cm^{-1}) 1695 (CO); ^1H NMR ($CDCl_3$, 200 MHz) δ 1.34 (t, 3H, J = 7.1 Hz, CH_3), 1.89−2.01 (m, 2H, CH_2), 2.73−2.87 (m, 4H, 2 × CH_2), 3.73 (s, 3H, CH_3), 4.32 (q, 2H, J = 7.1 Hz, CH_2), 6.05 (s, 2H, CH_2), 6.76 (d, 2H, J = 8.7 Hz, H-3′ and H-5′), 6.97 (d, 2H, J = 8.7 Hz, H-2′ and H-6′), 8.04 (s, 1H, H-3); ^{13}C NMR ($CDCl_3$, 50 MHz) δ 14.2, 23.1, 24.4, 25.3, 50.1, 55.2, 60.8, 113.8, 116.1, 120.3, 121.1, 123.9, 124.8, 127.6, 130.6, 151.8, 151.1, 158.6, 160.4. Anal. Calcd for $C_{21}H_{21}ClN_2O_4$: C, 62.92; H, 5.28; N, 6.99. Found: C, 62.99; H, 5.39; N, 6.93.

*Ethyl 7-Chloro-9-(2,5-dimethoxybenzyl)-4,5,6,9-tetrahydropyrrolo[2′,3′:3,4]cyclohepta[1,2-d][1,2]oxazole-8-carboxylate (**74**).* This compound was obtained from reaction of **65**. White solid; yield 68%; mp 147.2 °C; IR (cm^{-1}) 1696 (CO); ^1H NMR ($CDCl_3$, 200 MHz) δ 1.28 (t, 3H, J = 7.1 Hz, CH_3), 1.92−2.03 (m, 2H, CH_2), 2.77 (t, 2H, J = 6.0 Hz, CH_2), 2.86 (t, 2H, J = 6.0 Hz, CH_2), 3.62 (s, 3H, CH_3), 3.82 (s, 3H, CH_3), 4.27 (q, 2H, J = 7.1 Hz, CH_2), 5.98−6.06 (m, 3H, CH_2 and H-6′), 6.65 (dd, 1H, J = 8.8, 2.6 Hz, H-4′), 6.76 (d, 1H, J = 8.8 Hz, H-3′), 8.01 (s, 1H, H-3); ^{13}C NMR ($CDCl_3$, 50 MHz) δ 14.0, 23.1, 24.4, 25.3, 47.2, 55.5, 55.8, 60.7, 110.5, 110.7, 113.0, 115.9, 120.2, 121.3, 124.2, 124.5, 128.8, 150.6, 151.6, 153.4, 157.1, 160.0. Anal. Calcd for $C_{22}H_{23}ClN_2O_5$: C, 61.32; H, 5.38; N, 6.50. Found: C, 61.02; H, 5.52; N, 6.62.

*Ethyl 7-Chloro-9-(3,5-dimethoxybenzyl)-4,5,6,9-tetrahydropyrrolo[2′,3′:3,4]cyclohepta[1,2-d][1,2]oxazole-8-carboxylate (**75**).* This compound was obtained from reaction of **66**. White solid; yield 75%; mp 165.5 °C; IR (cm^{-1}) 1701 (CO); ^1H NMR ($CDCl_3$, 200 MHz) δ 1.26 (t, 3H, J = 7.1 Hz, CH_3), 1.94−2.03 (m, 2H, CH_2), 2.79 (t, 2H, J = 6.0 Hz, CH_2), 2.87 (t, 2H, J = 6.0 Hz,

https://dx.doi.org/10.1021/acs.jmedchem.0c01315
J. Med. Chem. 2020, 63, 12023−12042

CH_2), 3.58 (s, 3H, CH_3), 3.87 (s, 3H, CH_3), 4.21 (q, 2H, J = 7.1 Hz, CH_2), 5.50 (d, 1H, J = 2.6 Hz, H-2′), 6.13 (s, 2H, CH_2), 6.34 (d, 1H, J = 2.6 Hz, H-6′), 6.91 (s, 1H, H-4′), 7.99 (s, 1H, H-3); ^{13}C NMR ($CDCl_3$, 50 MHz) δ 14.2, 23.4, 24.5, 28.2, 49.1, 55.2, 56.2, 60.2, 97.2, 102.9, 111.7, 115.1, 119.1, 124.5, 125.7, 126.6, 139.2, 151.6, 155.7, 157.6, 158.9, 160.5. Anal. Calcd for $C_{22}H_{23}ClN_2O_5$: C, 61.32; H, 5.38; N, 6.50. Found: C, 61.36; H, 5.39; N, 6.29.

*8-Chloro-9-methyl-4,5,6,9-tetrahydropyrrolo[2′,3′:3,4]-cyclohepta[1,2-d][1,2]oxazole (**76**).* This compound was obtained from reaction of **52**. White solid; yield 62%; mp 66.9−67.2 °C; ^{1}H NMR ($CDCl_3$, 200 MHz) δ 1.87−1.99 (m, 2H, CH_2), 2.71−2.83 (m, 4H, 2 × CH_2), 3.92 (s, 3H, CH_3), 5.95 (s, 1H, H-7), 8.02 (s, 1H, H-3); ^{13}C NMR ($CDCl_3$, 50 MHz) δ 23.2, 24.3, 28.6, 33.6, 99.9, 108.4, 111.4, 120.2, 126.2, 151.5, 158.9. Anal. Calcd for $C_{11}H_{11}ClN_2O$: C, 59.33; H, 4.98; N, 12.58. Found: C, 59.28; H, 5.09; N, 12.71.

Biology. *Cell Lines and Compounds.* Established human cell lines derived from germinal center B-cell (GCB) (SU-DHL-10), activated B-cell (ABC) (HBL1) diffuse large B-cell lymphoma (DLBCL), mantle cell lymphoma (MCL) (MINO), splenic marginal zone lymphoma (SMZL) (parental VL51, VL51 idelalisib resistant clone, VL51 ibrutinib resistant clone) were cultured in culture RPMI-1640 media supplemented with fetal bovine serum (10%), penicillin−streptomycin−neomycin (~5,000 units of penicillin, 5 mg of streptomycinm and 10 mg of neomycin/mL, Sigma), and L-glutamine (1%). Vincristine sulfate was purchased from Sigma-Aldrich. Cell line identities were confirmed by CellCheck test (IDEXX, BioResearch, Ludwigsburg, Germany). All compounds were dissolved in dimethyl sulfoxide to obtain a stock concentration of 10 mM.

Cell Proliferation Analysis. The antiproliferative activity of all compounds was assessed by using the 3-(4.5-dimethylthiazolyl-2)-2,5-diphenyltetrazolium bromide (MTT) test. Cells were seeded in 96-well plates (nontissue culture treated) at a density of 1 × 10^5 cells/mL and treated with a single concentration of 1 μM for 72 h. Selected compounds that reached proliferation inhibition below 60% were further tested in order to calculate IC_{50} values. In this case, cells were treated in triplicate with serially diluted compounds in the appropriate tissue culture medium at a range of 40−10 000 nM. Cells were incubated for 72 h at 37 °C, 5% CO_2. Wells containing medium only were included on each plate and served as blanks for absorbance readings. MTT (Sigma, Buchs, Switzerland) was prepared as a 5 mg/mL stock solution in phosphate buffered saline (PBS) and filter-sterilized. MTT solution (22 μL) was added to each well, and tissue culture plates were incubated at 37 °C for 4 h. Cells were then lysed with 25% sodium dodecyl sulfate lysis buffer, and absorbance was read at 570 nm using a Beckman Coulter-AD340 plate reader.

Evaluation of Cytotoxicity in PBLs. PBLs were obtained from human peripheral blood (leucocyte rich plasma-buffy coats) from healthy volunteers using the Lymphoprep (Fresenius KABI Norge AS) gradient density centrifugation.

Buffy coats were obtained from the Blood Transfusion Service, Azienda Ospedaliera of Padova and provided at this institution for research purposes. Therefore, no further informed consent was needed. In addition, buffy coats were provided without identifiers. The experimental procedures were carried out in strict accordance with approved guidelines.

After extensive washing, cells were resuspended (1.0 × 10^6 cells/mL) in RPMI-1640 with 10% fetal bovine serum and incubated overnight. For cytotoxicity evaluations in proliferating PBL cultures, nonadherent cells were resuspended at 5 × 10^5 cells/mL in growth medium, containing 2.5 μg/mL PHA (Irvine Scientific). Different concentrations of the test compounds were added, and viability was determined 72 h later by the MTT test. For cytotoxicity evaluations in resting PBL cultures, nonadherent cells were resuspended (5 × 10^5 cells/mL) and treated for 72 h with the test compounds.

Tubulin Studies. Electrophoretically pure bovine brain tubulin was obtained as described previously.[70] Analysis of effects on tubulin polymerization was performed by turbidimetry at 350 nm in recording spectrophotometers equipped with electronic temperature controllers as described in detail elsewhere.[71] The tubulin used in these studies was more active than that used in ref 71, and so the concentration of tubulin was reduced from 10 to 9 μM (1.0 to 0.9 mg/mL) and the concentration of GTP from 0.4 to 0.2 mM. This was done to obtain an IC_{50} for CA-4, the reference compound, similar to that obtained in ref 71. The binding of [^{3}H]colchicine to tubulin was perfomed as described in detail previously[72] except that the tubulin concentration was reduced from 0.1 mg/mL to 0.05 mg/mL and only one, instead of two, DEAE-cellulose filter was used for each reaction mixture.

Flow Cytometric Analysis of Cell Cycle Distribution. 5 ×10^5 HeLa cells were treated with different concentrations of the test compounds for 24 h. After the incubation period, the cells were collected, centrifuged, and fixed with ice-cold ethanol (70%). The cells were treated with lysis buffer containing RNase A and 0.1% Triton X-100 and stained with PI. Samples were analyzed on a Cytomic FC500 flow cytometer (Beckman Coulter). DNA histograms were analyzed using MultiCycle for Windows (Phoenix Flow Systems).

Apoptosis Assay. Cell death was determined by flow cytometry of cells double stained with annexin V/FITC and PI. The Coulter Cytomics FC500 (Beckman Coulter) was used to measure the surface exposure of phosphatidylserine on apoptotic cells according to the manufacturer's instructions (Annexin-V Fluos, Roche Diagnostics).

Assessment of Mitochondrial Potential and ROS. The mitochondrial membrane potential was measured with the lipophilic cationic dye 5,5′,6,6′ tetrachlo-1,1′,3,3′-tetraethylbenzimidazolcarbocyanine (JC-1) (Molecular Probes), as described.[73] The method is based on the ability of this fluorescent probe to enter selectively into mitochondria since it changes reversibly its color from green to red as membrane potential increases. This property is due to the reversible formation of JC-1 aggregates upon membrane polarization that causes a shift in the emitted light from 530 nm (i.e., emission of JC-1 monomeric form) to 590 nm (emission of JC-1-aggregate) when excited at 490 nm.

The production of ROS was measured by flow cytometry using H_2DCFDA (Molecular Probes), as previously described.[59] Briefly, after different times of treatment, cells were collected by centrifugation and resuspended in PBS containing H_2DCFDA at the concentration of 0.1 μM. The cells were then incubated for 30 min at 37 °C, centrifuged, and resuspended in PBS. The fluorescence was directly recorded with the flow cytometer, using as excitation wavelength 488 nm and emission at 530 nm.

Western Blot Analysis. HeLa cells were incubated in the presence of the test compound and, after different times, were collected, centrifuged, and washed two times with ice cold PBS. The pellet was resuspended in lysis buffer. After the cells were lysed on ice for 30 min, lysates were centrifuged at 15 000g at 4 °C for 10 min. The protein concentration in the supernatant was determined using the BCA protein assay reagents (Pierce, Italy). Equal amounts of protein (10 μg) were resolved using sodium dodecyl sulfate−polyacrylamide gel electrophoresis (Criterion Precast, BioRad, Italy) and transferred to a PVDF Hybond-P membrane (GE Healthcare). Membranes were blocked with a bovine serum albumin solution (5% in Tween PBS 1×), and the membranes were gently rotated overnight at 4 °C in the albumin solution. Membranes were then incubated with primary antibodies against PARP cleaved fragment, cdc25c, cyclin B, p-cdc2^{Tyr15}, XIAP, and Mcl-1 (all from Cell Signaling) or GAPDH (Sigma-Aldrich) for 2 h at room temperature. Membranes were next incubated with peroxidase labeled secondary antibodies for 1 h. All membranes were visualized using ECL Select (GE Healthcare), and images were acquired using an Uvitec-Alliance imaging system (Uvitec, Cambridge, U.K.). To ensure equal protein loading, each membrane was stripped and reprobed with anti-GAPDH antibody. To obtain relative quantitative data, ImageJ software (NIH, USA) was used for scanning densitometry analysis of Western blots.

Molecular Modeling. *Docking Studies.* All molecular modeling simulations were carried out using the Schrödinger Suite version 2018.[74] In particular, the LigPrep tool[75] was used to model the 3D structure of each ligand, to calculate and to energy minimize their protonation state at pH 7.4 using OPLS_2005 as force field.[76] First, docking studies of new derivatives were performed by using three different crystal structures of tubulin, characterized by two dimers of $\alpha-\beta$ tubulin heterodimers, downloaded from the Protein Data Bank

https://dx.doi.org/10.1021/acs.jmedchem.0c01315
J. Med. Chem. 2020, 63, 12023−12042

(PDB).[77] Models having PDB codes 4O2B and 1Z2B were selected as colchicine-bound[78] and vinblastine-bound[79] cocrystal structures, respectively. According to literature data, the tubulin colchicine domain consists of the main site, where colchicine binds (zone 1), and two additional neighboring pockets (zones 2 and 3).[80] To better discriminate the most likely binding area of the new derivatives, in addition to the 4O2B structure, representing the colchicine-like binding site area (zones 1 and 2), the model with PDB code 3N2G,[80] cocrystallized with the inhibitor G2N, was also used in docking studies to represent the binding zones 2 and 3. Each X-ray model was preprocessed using the Protein Preparation Wizard tool and the OPLS_2005 force field, in order to add hydrogen atoms, to assign partial charges and to build missing atoms, side chains, and loops. The nucleotides (GTP and GDP) and the metals (Mg^{2+} and Zn^{2+}) were retained during the docking calculations, while all water molecules were removed. Thus, the docking grids were prepared using as centroid the cocrystallized ligands (i.e., colchicine for 1SA0, vinblastine for 1Z2B, and G2N for 3N2G), while box size and position were generated automatically. Docking studies were performed by using the software Glide version 7.8[81] and by applying the Glide Extra-Precision (XP) protocol, selected after redocking analysis (for details, see Supporting Information paragraph "Redocking Analysis" and Table S1). Ten poses per ligand were taken into account, and the default docking scoring function was used for selecting the best binding mode for each ligand. To perform the following computational studies, for each tubulin crystal structure only one α-tubulin and one β-tubulin structure were selected, specifically the C and D chains for 4O2B, the B and C chains for 1Z2B, and the A and B chains for 3N2G, with respect to the redocking analysis.

Molecular Dynamics Simulations (MDs). To better characterize the binding mode of our best active compounds (**57**, **58**, **63**, **66**, **67**, **75**, and **3**), their complexes with the 4O2B model were subjected to molecular dynamics simulations (MDs). The Desmond package[82] was used for MDs, employing OPLS_2005 as force field in an explicit solvent (TIP3 water model).[83] The best docking pose for each single compound was taken as initial coordinates for the MDs. An orthorhombic water box was built for the solvation of the system, ensuring a buffer distance of approximately 10 Å between each box side and the complex atoms. The system was neutralized by adding K^+ counterions, and it was minimized and pre-equilibrated using the default relaxation routine implemented in Desmond. Simulation time was set to 20 ns, under *NPT* conditions at 1 atm and 300 K, with a recording interval equal to 40 ps. The time step was set to 2 fs. MD analyses were performed using the Simulation Event Analysis tool of Desmond, while visualization of each protein−ligand complex was carried out using Maestro. For each compound, average ligand RMSD value was calculated on their heavy atoms by first aligning the complex on the protein backbone of the reference structure. Moreover, by use of the Desmond Trajectory Clustering tool, the best representative structure of the whole MDs was generated in order to examine the possibility of induced-fit binding events of our compounds. Finally, these selected structures were submitted to the calculation of the ΔG_{bind} value by using the MM/GBSA method as implemented in the Prime module[84] from Maestro using the default settings.

Statistical Analysis. The differences between different treatments were analyzed, using the two-sided Student's *t* test. *P* values lower than 0.05 were considered significant.

■ ASSOCIATED CONTENT

Supporting Information

The Supporting Information is available free of charge at https://pubs.acs.org/doi/10.1021/acs.jmedchem.0c01315.

Figures S1−S4 showing dose−response curves and mean graph midpoints of compounds **66** and **67**; Table S1 listing RMSD (Å) and G-Score (kcal/mol) values, obtained by means of Glide Extra-Precision (XP), for each chain in the dimer used in the crystallographic structures used in computational simulations; Table S2 listing G-Score (kcal/mol) values for the best poses of all compounds complexed with both the 4O2B and 1Z2B crystallographic structures; Table S3 listing G-Score values, expressed as kcal/mol, of the best active compounds **57**, **58**, **63**, **66**, **67**, **75**, and **3** against both the 4O2B and 3N2G crystallographic structures; Figure S5 showing the best-docked poses of **57**, **58**, **63**, **66**, **67**, **75**, and **3** against the crystal structure of tubulin with the PDB code 3N2G, depicting zones 2 and 3 of the colchicine site; geometric and energetic analysis of molecular dynamics simulations (MDs); Table S4 listing representative structures of MDs, number of contacts, and binding energy; Figures S6−S31 showing NMR spectra of compounds **51**−**76**; HPLC traces of compounds **66** and **67** (PDF)

PDB files (ZIP)

Accession Codes

The PDB code for cocrystal structure of tubulin with colchicine is 4O2B. The PDB code for cocrystal structure of tubulin with vinblastine is 1Z2B. The PDB code for cocrystal structure of tubulin with inhibitor G2N is 3N2G.

■ AUTHOR INFORMATION

Corresponding Author

Alessandra Montalbano − *Department of Biological, Chemical and Pharmaceutical Sciences and Technologies (STEBICEF), University of Palermo, 90123 Palermo, Italy;* orcid.org/0000-0002-8891-598X; Phone: +39-091-6161606; Email: alessandra.montalbano@unipa.it

Authors

Virginia Spanò − *Department of Biological, Chemical and Pharmaceutical Sciences and Technologies (STEBICEF), University of Palermo, 90123 Palermo, Italy*

Roberta Rocca − *Net4Science srl, Academic Spinoff, Università Magna Græcia di Catanzaro, 88100 Catanzaro, Italy; Dipartimento di Medicina Sperimentale e Clinica, Università Magna Græcia di Catanzaro, 88100 Catanzaro, Italy;* orcid.org/0000-0002-0680-7097

Marilia Barreca − *Department of Biological, Chemical and Pharmaceutical Sciences and Technologies (STEBICEF), University of Palermo, 90123 Palermo, Italy; Institute of Oncology Research, Faculty of Biomedical Sciences, Università della Svizzera Italiana, 6500 Bellinzona, Switzerland*

Daniele Giallombardo − *Department of Biological, Chemical and Pharmaceutical Sciences and Technologies (STEBICEF), University of Palermo, 90123 Palermo, Italy*

Anna Carbone − *Department of Biological, Chemical and Pharmaceutical Sciences and Technologies (STEBICEF), University of Palermo, 90123 Palermo, Italy*

Maria Valeria Raimondi − *Department of Biological, Chemical and Pharmaceutical Sciences and Technologies (STEBICEF), University of Palermo, 90123 Palermo, Italy*

Eugenio Gaudio − *Institute of Oncology Research, Faculty of Biomedical Sciences, Università della Svizzera Italiana, 6500 Bellinzona, Switzerland*

Roberta Bortolozzi − *Istituto di Ricerca Pediatrica IRP, Fondazione Città della Speranza, 35127 Padova, Italy*

Ruoli Bai − *Screening Technologies Branch, Developmental Therapeutics Program, Division of Cancer Treatment and Diagnosis, Frederick National Laboratory for Cancer Research,*

National Cancer Institute, National Institutes of Health, Frederick, Maryland 21702, United States

Pierfrancesco Tassone − *Dipartimento di Medicina Sperimentale e Clinica, Università Magna Græcia di Catanzaro, 88100 Catanzaro, Italy*

Stefano Alcaro − *Dipartimento di Scienze della Salute, Università Magna Græcia di Catanzaro, 88100 Catanzaro, Italy; Net4Science srl, Academic Spinoff, Università Magna Græcia di Catanzaro, 88100 Catanzaro, Italy*

Ernest Hamel − *Screening Technologies Branch, Developmental Therapeutics Program, Division of Cancer Treatment and Diagnosis, Frederick National Laboratory for Cancer Research, National Cancer Institute, National Institutes of Health, Frederick, Maryland 21702, United States*

Giampietro Viola − *Istituto di Ricerca Pediatrica IRP, Fondazione Città della Speranza, 35127 Padova, Italy; Dipartimento di Salute della Donna e del Bambino, Laboratorio di Oncoematologia, Università di Padova, 35131 Padova, Italy*

Francesco Bertoni − *Institute of Oncology Research, Faculty of Biomedical Sciences, Università della Svizzera Italiana, 6500 Bellinzona, Switzerland; Oncology Institute of Southern Switzerland, 6500 Bellinzona, Switzerland*

Paola Barraja − *Department of Biological, Chemical and Pharmaceutical Sciences and Technologies (STEBICEF), University of Palermo, 90123 Palermo, Italy*

Complete contact information is available at: https://pubs.acs.org/10.1021/acs.jmedchem.0c01315

Author Contributions

◇V.S., R.R., and M.B. contributed equally.

Notes

The authors declare no competing financial interest.

■ ACKNOWLEDGMENTS

This work was financially supported by the Ministero dell'Istruzione, dell'Università e della Ricerca (MIUR). This research was supported in part by the Developmental Therapeutics Program in the Division of Cancer Treatment and Diagnosis of the National Cancer Institute, which includes federal funds under Contract HHSN261200800001E. The content of this publication does not necessarily reflect the views or policies of the Department of Health and Human Services, nor does mention of trade names, commercial products, or organizations imply endorsement by the U.S. Government. The authors also thank the Developmental Therapeutic Program of the National Cancer Institute for performing cytoxicity studies with selected compounds in the 60 cancer cell line screen. The authors also acknowledge the Italian Association for Cancer Research (AIRC) research project "Small molecule-based targeting of lncRNAs 3D structure: a translational platform for the treatment of multiple myeloma" (Code 21588), the PRIN 2017 research project "Novel anticancer agents endowed with multi-targeting mechanism of action" (Code 201744BN5T), and the PRIN 2017 research project "Selective mGlu3 metabotropic glutamate receptor ligands as new potential therapeutic agents in experimental models of parkinsonism" (Code 2017XZ7A37) funded by the Italian MIUR.

■ ABBREVIATIONS USED

NCI, National Cancer Istitute; FDA, Food and Drug Administration; CA-4, combretastatin A-4; CA-4P, combretastatin A-4 phosphate disodium; MDR, multidrug resistance; MG_MID, mean graph midpoint; DMPM, diffuse malignant peritoneal mesothelioma; DMF, *N*,*N*-dimethylformamide; DMFDMA, *N*,*N*-dimethylformamide dimethyl acetal; MW, microwave; TBDMAM, *tert*-butoxy bis(dimethylamino)-methane; PI3Kδ, phosphatidylinositol 3-kinase-δ; BTK, Bruton's tyrosine kinase; MZL, marginal zone lymphoma; MCL, mantle cell lymphoma; ABC DLBCL, activated B-cell-like diffuse large B cell lymphoma; GCB DLBCL, germinal center B-cell type diffuse large B cell lymphoma; PBL, peripheral blood lymphocyte; PHA, phytohematoaglutinin; RMSD, root-mean-square deviation; MDs, molecular dynamics simulations; PI, propidium iodide; ROS, reactive oxygen species; H_2-DCFDA, 2,7-dichlorodihydrofluorescein diacetate; DCF, dichlorofluorescein; PARP, poly(ADP)ribose polymerase; DMSO, dimethyl sulfoxide; s, singlet; d, doublet; t, triplet; q, quartet; m, multiplet; TIC, total ion current.

■ REFERENCES

(1) Preti, D.; Romagnoli, R.; Rondanin, R.; Cacciari, B.; Hamel, E.; Balzarini, J.; Liekens, S.; Schols, D.; Estévez-Sarmiento, F.; Quintana, J.; Estevez, F. Design, synthesis, in vitro antiproliferative activity and apoptosis-inducing studies of 1-(3′,4′,5′-trimethoxyphenyl)-3-(2′-alkoxycarbonylindolyl)-2-propen-1-one derivatives obtained by a molecular hybridisation approach. *J. Enzyme Inhib. Med. Chem.* **2018**, *33* (1), 1225−1238.

(2) Akhmanova, A.; Steinmetz, M. O. Control of microtubule organization and dynamics: two ends in the limelight. *Nat. Rev. Mol. Cell Biol.* **2015**, *16* (12), 711−726.

(3) Jordan, M. A.; Wilson, L. Microtubules as a target for anticancer drugs. *Nat. Rev. Cancer* **2004**, *4*, 253−265.

(4) Seddigi, Z. S.; Malik, M. S.; Saraswati, A. P.; Ahmed, S. A.; Babalghith, A. O.; Lamfon, H. A.; Kamal, A. Recent advances in combretastatin based derivatives and prodrugs as antimitotic agents. *MedChemComm* **2017**, *8* (8), 1592−1603.

(5) Li, W.; Xu, F.; Shuai, W.; Sun, H.; Yao, H.; Ma, C.; Xu, S.; Yao, H.; Zhu, Z.; Yang, D. H.; Chen, Z.-S.; Xu, J. Discovery of novel quinoline-chalcone derivatives as potent antitumor agents with microtubule polymerization inhibitory activity. *J. Med. Chem.* **2019**, *62* (2), 993−1013.

(6) Prasad, B.; Lakshma Nayak, V.; Srikanth, P. S.; Baig, M. F.; Subba Reddy, N. V.; Babu, K. S.; Kamal, A. Synthesis and biological evaluation of 1-benzyl-*N*-(2-(phenylamino)pyridin-3-yl)-1*H*-1,2,3-triazole-4-carboxamides as antimitotic agents. *Bioorg. Chem.* **2019**, *83*, 535−548.

(7) Lu, Y.; Chen, J.; Xiao, M.; Li, W.; Miller, D. D. An overview of tubulin inhibitors that interact with the colchicine binding site. *Pharm. Res.* **2012**, *29* (11), 2943−2971.

(8) Guo, H.; Li, X.; Guo, Y.; Zhen, L. An overview of tubulin modulators deposited in Protein Data Bank. *Med. Chem. Res.* **2019**, *28* (7), 927−937.

(9) Tron, G. C.; Pirali, T.; Sorba, G.; Pagliai, F.; Busacca, S.; Genazzani, A. A. Medicinal chemistry of combretastatin A4: present and future directions. *J. Med. Chem.* **2006**, *49* (11), 3033−3044.

(10) Pettit, G. R.; Singh, S. B.; Boyd, M. R.; Hamel, E.; Pettit, R. K.; Schmidt, J. M.; Hogan, F. Antineoplastic Agents 291. Isolation and synthesis of combretastatins A-4, A-5, and A-6. *J. Med. Chem.* **1995**, *38* (10), 1666−1672.

(11) Subba Rao, A. V.; Swapna, K.; Shaik, S. P.; Lakshma Nayak, V.; Srinivasa Reddy, T.; Sunkari, S.; Shaik, T. B.; Bagul, C.; Kamal, A. Synthesis and biological evaluation of *cis*-restricted triazole/tetrazole mimics of combretastatin-benzothiazole hybrids as tubulin polymerization inhibitors and apoptosis inducers. *Bioorg. Med. Chem.* **2017**, *25* (3), 977−999.

(12) Pérez-Pérez, M. J.; Priego, E. M.; Bueno, O.; Martins, M. S.; Canela, M. D.; Liekens, S. Blocking blood flow to solid tumors by

destabilizing tubulin: an approach to targeting tumor growth. *J. Med. Chem.* **2016**, *59* (19), 8685−8711.
(13) Young, S. L.; Chaplin, D. J. Combretastatin A4 phosphate: background and current clinical status. *Expert Opin. Invest. Drugs* **2004**, *13* (9), 1171−1181.
(14) Bailly, C.; Bal, C.; Barbier, P.; Combes, S.; Finet, J. P.; Hildebrand, M. P.; Peyrot, V.; Wattez, N. Synthesis and biological evaluation of 4-arylcoumarin analogues of combretastatins. *J. Med. Chem.* **2003**, *46* (25), 5437−5444.
(15) Rappl, C.; Barbier, P.; Bourgarel-Rey, V.; Grégoire, C.; Gilli, R.; Carre, M.; Combes, S.; Finet, J. P.; Peyrot, V. Interaction of 4-arylcoumarin analogues of combretastatins with microtubule network of HBL100 cells and binding to tubulin. *Biochemistry* **2006**, *45* (30), 9210−9218.
(16) Sun, C. M.; Lin, L. G.; Yu, H. J.; Cheng, C. Y.; Tsai, Y. C.; Chu, C. W.; Din, Y. H.; Chau, Y. P.; Don, M. J. Synthesis and cytotoxic activities of 4,5-diarylisoxazoles. *Bioorg. Med. Chem. Lett.* **2007**, *17* (4), 1078−1081.
(17) Kaffy, J.; Pontikis, R.; Carrez, D.; Croisy, A.; Monneret, C.; Florent, J. C. Isoxazole-type derivatives related to combretastatin A-4, synthesis and biological evaluation. *Bioorg. Med. Chem.* **2006**, *14* (12), 4067−4077.
(18) Shin, K. D.; Yoon, Y. J.; Kang, Y. R.; Son, K. H.; Kim, H. M.; Kwon, B. M.; Han, D. C. KRIBB3, a novel microtubule inhibitor, induces mitotic arrest and apoptosis in human cancer cells. *Biochem. Pharmacol.* **2008**, *75* (2), 383−394.
(19) Lee, S.; Kim, J. N.; Lee, H. K.; Yoon, K. S.; Shin, K. D.; Kwon, B. M.; Han, D. C. Biological evaluation of KRIBB3 analogs as a microtubule polymerization inhibitor. *Bioorg. Med. Chem. Lett.* **2011**, *21* (3), 977−979.
(20) Zhu, J.; Mo, J.; Lin, H.; Chen, Y.; Sun, H. The recent progress of isoxazole in medicinal chemistry. *Bioorg. Med. Chem.* **2018**, *26* (12), 3065−3075.
(21) Yoon, H.; Kwak, Y.; Choi, S.; Cho, H.; Kim, N. D.; Sim, T. A pyrazolo[3,4-*d*]pyrimidin-4-amine derivative containing an isoxazole moiety is a selective and potent inhibitor of RET gatekeeper mutants. *J. Med. Chem.* **2016**, *59* (1), 358−373.
(22) Sharma, R.; Jain, A.; Sahu, B.; Singh, D.; Mali, S. Heterocyclyl Compounds and Uses Thereof. WO2014181287, 2014.
(23) Yu, L. F.; Tückmantel, W.; Eaton, J. B.; Caldarone, B.; Fedolak, A.; Hanania, T.; Brunner, D.; Lukas, R. J.; Kozikowski, A. P. Identification of novel A4β2-nicotinic acetylcholine receptor (NAChR) agonists based on an isoxazole ether scaffold that demonstrate antidepressant-like activity. *J. Med. Chem.* **2012**, *55* (2), 812−823.
(24) Yermolina, M. V.; Wang, J.; Caffrey, M.; Rong, L. L.; Wardrop, D. J. Discovery, synthesis, and biological evaluation of a novel group of selective inhibitors of filoviral entry. *J. Med. Chem.* **2011**, *54* (3), 765−781.
(25) Deng, B. L.; Hartman, T. L.; Buckheit, R. W.; Pannecouque, C.; De Clercq, E.; Cushman, M. Replacement of the metabolically labile methyl esters in the alkenyldiarylmethane series of non-nucleoside reverse transcriptase inhibitors with isoxazolone, isoxazole, oxazolone, or cyano substituents. *J. Med. Chem.* **2006**, *49* (17), 5316−5323.
(26) Patel, N. C.; Schwarz, J.; Hou, X. J.; Hoover, D. J.; Xie, L.; Fliri, A. J.; Gallaschun, R. J.; Lazzaro, J. T.; Bryce, D. K.; Hoffmann, W. E.; Hanks, A. N.; McGinnis, D.; Marr, E. S.; Gazard, J. L.; Hajós, M.; Scialis, R. J.; Hurst, R. S.; Shaffer, C. L.; Pandit, J.; O'Donnell, C. J. Discovery and characterization of a novel dihydroisoxazole class of α-amino-3-hydroxy-5-methyl-4-isoxazolepropionic acid (AMPA) receptor potentiators. *J. Med. Chem.* **2013**, *56* (22), 9180−9191.
(27) Velaparthi, S.; Brunsteiner, M.; Uddin, R.; Wan, B.; Franzblau, S. G.; Petukhov, P. A. 5-*Tert*-butyl-*N*-pyrazol-4-yl-4,5,6,7-tetrahydrobenzo[*d*]isoxazole-3-carboxamide derivatives as novel potent inhibitors of mycobacterium tuberculosis pantothenate synthetase: initiating a quest for new antitubercular drugs. *J. Med. Chem.* **2008**, *51* (7), 1999−2002.
(28) Sysak, A.; Obmińska-Mrukowicz, B. Isoxazole ring as a useful scaffold in a search for new therapeutic agents. *Eur. J. Med. Chem.* **2017**, *137*, 292−309.
(29) Mahboobi, S.; Pongratz, H.; Hufsky, H.; Hockemeyer, J.; Frieser, M.; Lyssenko, A.; Paper, D. H.; Bürgermeister, J.; Böhmer, F. D.; Fiebig, H. H.; Burger, A. M.; Baasner, S.; Beckers, T. Synthetic 2-aroylindole derivatives as a new class of potent tubulin-inhibitory, antimitotic agents. *J. Med. Chem.* **2001**, *44* (26), 4535−4553.
(30) Beckers, T.; Reissmann, T.; Schmidt, M.; Fiebig, H. H.; Burger, A. M.; Vanhoefer, U.; Mahboobi, S.; Pongratz, H.; Hockemeyer, J.; Frieser, M.; Mahboobi, S. 2-Aroylindoles, a novel class of potent, orally active small molecule tubulin inhibitors. *Cancer Res.* **2002**, *62* (11), 3113−3119.
(31) Putey, A.; Popowycz, F.; Do, Q. T.; Bernard, P.; Talapatra, S. K.; Kozielski, F.; Galmarini, C. M.; Joseph, B. Indolobenzazepin-7-ones and 6-, 8-, and 9-membered ring derivatives as tubulin polymerization inhibitors: synthesis and structure-activity relationship studies. *J. Med. Chem.* **2009**, *52* (19), 5916−5925.
(32) Hadimani, M. B.; MacDonough, M. T.; Ghatak, A.; Strecker, T. E.; Lopez, R.; Sriram, M.; Nguyen, B. L.; Hall, J. J.; Kessler, R. J.; Shirali, A. R.; Liu, L.; Garner, C. M.; Pettit, G. R.; Hamel, E.; Chaplin, D. J.; Mason, R. P.; Trawick, M. L.; Pinney, K. G. Synthesis of a 2-aryl-3-aroyl indole salt (OXi8007) resembling combretastatin A-4 with application as a vascular disrupting agent. *J. Nat. Prod.* **2013**, *76* (9), 1668−1678.
(33) Diana, P.; Stagno, A.; Barraja, P.; Montalbano, A.; Carbone, A.; Parrino, B.; Cirrincione, G. Synthesis of the new ring system pyrrolizino[2,3-*b*]indol-4(5*H*)-one. *Tetrahedron* **2011**, *67* (19), 3374−3379.
(34) Diana, P.; Stagno, A.; Barraja, P.; Carbone, A.; Parrino, B.; Dall'Acqua, F.; Vedaldi, D.; Salvador, A.; Brun, P.; Castagliuolo, I.; Issinger, O. G.; Cirrincione, G. Synthesis of triazenoazaindoles: a new class of triazenes with antitumor activity. *ChemMedChem* **2011**, *6* (7), 1291−1299.
(35) Barraja, P.; Spanò, V.; Patrizia, D.; Carbone, A.; Cirrincione, G.; Vedaldi, D.; Salvador, A.; Viola, G.; Dall'Acqua, F. Pyrano[2,3-*e*]isoindol-2-ones, new angelicin heteroanalogues. *Bioorg. Med. Chem. Lett.* **2009**, *19* (6), 1711−1714.
(36) Spanò, V.; Montalbano, A.; Carbone, A.; Scudieri, P.; Galietta, L. J. V.; Barraja, P. An overview on chemical structures as ΔF508-CFTR correctors. *Eur. J. Med. Chem.* **2019**, *180*, 430−448.
(37) Pojero, F.; Poma, P.; Spanò, V.; Montalbano, A.; Barraja, P.; Notarbartolo, M. Targeting multiple myeloma with natural polyphenols. *Eur. J. Med. Chem.* **2019**, *180*, 465−485.
(38) Barraja, P.; Diana, P.; Lauria, A.; Montalbano, A.; Almerico, A. M.; Dattolo, G.; Cirrincione, G.; Viola, G.; Dall'Acqua, F. Pyrrolo[2,3-*h*]quinolinones: synthesis and photochemotherapic activity. *Bioorg. Med. Chem. Lett.* **2003**, *13* (16), 2809−2811.
(39) Diana, P.; Barraja, P.; Lauria, A.; Montalbano, A.; Almerico, A. M.; Dattolo, G.; Cirrincione, G. Pyrrolo[2,1-*d*][1,2,3,5]tetrazine-4(3*H*)-ones, a new class of azolotetrazines with potent antitumor activity. *Bioorg. Med. Chem.* **2003**, *11* (11), 2371−2380.
(40) Whatmore, J. L.; Swann, E.; Barraja, P.; Newsome, J. J.; Bunderson, M.; Beall, H. D.; Tooke, J. E.; Moody, C. J. Comparative study of isoflavone, quinoxaline and oxindole families of anti-angiogenic agents. *Angiogenesis* **2002**, *5* (1−2), 45−51.
(41) Almerico, A. M.; Mingoia, F.; Diana, P.; Barraja, P.; Montalbano, A.; Lauria, A.; Loddo, R.; Sanna, L.; Delpiano, D.; Setzu, M. G.; Musiu, C. Pyrrolo[1,2-*f*]phenanthridines and related non-rigid analogues as antiviral agents. *Eur. J. Med. Chem.* **2002**, *37* (1), 3−10.
(42) Barraja, P.; Spanò, V.; Giallombardo, D.; Diana, P.; Montalbano, A.; Carbone, A.; Parrino, B.; Cirrincione, G. Synthesis of [1,2]oxazolo[5,4-*e*]indazoles as antitumour agents. *Tetrahedron* **2013**, *69* (31), 6474−6477.
(43) Barraja, P.; Caracausi, L.; Diana, P.; Spanò, V.; Montalbano, A.; Carbone, A.; Parrino, B.; Cirrincione, G. Synthesis and antiproliferative activity of the ring system [1,2]oxazolo[4,5-*g*]indole. *ChemMedChem* **2012**, *7* (11), 1901−1904.

https://dx.doi.org/10.1021/acs.jmedchem.0c01315
J. Med. Chem. 2020, 63, 12023−12042

(44) Spano, V.; Pennati, M.; Parrino, B.; Carbone, A.; Montalbano, A.; Cilibrasi, V.; Zuco, V.; Lopergolo, A.; Cominetti, D.; Diana, P.; Cirrincione, G.; Barraja, P.; Zaffaroni, N. Preclinical activity of new [1,2]oxazolo[5,4-*e*]isoindole derivatives in diffuse malignant peritoneal mesothelioma. *J. Med. Chem.* **2016**, *59* (15), 7223−7238.
(45) Spanò, V.; Pennati, M.; Parrino, B.; Carbone, A.; Montalbano, A.; Lopergolo, A.; Zuco, V.; Cominetti, D.; Diana, P.; Cirrincione, G.; Zaffaroni, N.; Barraja, P. [1,2]Oxazolo[5,4-*e*]isoindoles as promising tubulin polymerization inhibitors. *Eur. J. Med. Chem.* **2016**, *124*, 840−851.
(46) Sriram, M.; Hall, J. J.; Grohmann, N. C.; Strecker, T. E.; Wootton, T.; Franken, A.; Trawick, M. L.; Pinney, K. G. Design, synthesis and biological evaluation of dihydronaphthalene and benzosuberene analogs of the combretastatins as inhibitors of tubulin polymerization in cancer chemotherapy. *Bioorg. Med. Chem.* **2008**, *16* (17), 8161−8171.
(47) Tanpure, R. P.; George, C. S.; Strecker, T. E.; Devkota, L.; Tidmore, J. K.; Lin, C. M.; Herdman, C. A.; Macdonough, M. T.; Sriram, M.; Chaplin, D. J.; Trawick, M. L.; Pinney, K. G. Synthesis of structurally diverse benzosuberene analogues and their biological evaluation as anti-cancer agents. *Bioorg. Med. Chem.* **2013**, *21* (24), 8019−8032.
(48) Spanò, V.; Frasson, I.; Giallombardo, D.; Doria, F.; Parrino, B.; Carbone, A.; Montalbano, A.; Nadai, M.; Diana, P.; Cirrincione, G.; Freccero, M.; Richter, S. N.; Barraja, P. Synthesis and antiproliferative mechanism of action of pyrrolo[3′,2′:6,7]cyclohepta[1,2-*d*]pyrimidin-2-amines as singlet oxygen photosensitizers. *Eur. J. Med. Chem.* **2016**, *123*, 447−461.
(49) Spanò, V.; Giallombardo, D.; Cilibrasi, V.; Parrino, B.; Carbone, A.; Montalbano, A.; Frasson, I.; Salvador, A.; Richter, S. N.; Doria, F.; Freccero, M.; Cascioferro, S.; Diana, P.; Cirrincione, G.; Barraja, P. Pyrrolo[3′,2′:6,7]cyclohepta[1,2-*b*]pyridines with potent photo-antiproliferative activity. *Eur. J. Med. Chem.* **2017**, *128*, 300−318.
(50) Monks, A.; Scudiero, D.; Skehan, P.; Shoemaker, R.; Paull, K.; Vistica, D.; Hose, C.; Langley, J.; Cronise, P.; Vaigro-Wolff, A.; Gray-Goodrich, M.; Campbell, H.; Mayo, J.; Boyd, M. Feasibility of a high-flux anticancer drug screen using a diverse panel of cultured human tumor cell lines. *J. Natl. Cancer Inst.* **1991**, *83* (11), 757−766.
(51) Arribas, A. J.; Napoli, S.; Gaudio, E.; Cascione, L.; Di Veroli, A.; Tarantelli, C.; Spriano, F.; Zucchetto, A.; Rossi, F. M.; Rinaldi, A.; Stathis, A.; Stuessi, G.; Gattei, V.; Cruciani, G.; Zucca, E.; Rossi, D.; Bertoni, F. Secreted factors determine resistance to idelalisib in marginal zone lymphoma models of resistance. *Blood* **2019**, *134*, 2569.
(52) Arribas, A. J.; Napoli, S.; Gaudio, E.; Cascione, L.; Di Veroli, A.; Tarantelli, C.; Spriano, F.; Zucchetto, A.; Rossi, F.; Sartori, G.; Rinaldi, A.; Stathis, A.; Stussi, G.; Gattei, V.; Cruciani, G.; Zucca, E.; Rossi, D.; Bertoni, F. Abstract A127: Secretion of IL16 is associated with resistance to ibrutinib in pre-clinical models of lymphoma. *Mol. Cancer Ther.* **2019**, *18*, A127.
(53) Romagnoli, R.; Baraldi, P. G.; Kimatrai Salvador, M.; Preti, D.; Aghazadeh Tabrizi, M.; Bassetto, M.; Brancale, A.; Hamel, E.; Castagliuolo, I.; Bortolozzi, R.; Basso, G.; Viola, G. Synthesis and biological evaluation of 2-(alkoxycarbonyl)-3-anilinobenzo[*b*]-thiophenes and thieno[2,3-*b*]pyridines as new potent anticancer agents. *J. Med. Chem.* **2013**, *56* (6), 2606−2618.
(54) Romagnoli, R.; Baraldi, P. G.; Salvador, M. K.; Prencipe, F.; Bertolasi, V.; Cancellieri, M.; Brancale, A.; Hamel, E.; Castagliuolo, I.; Consolaro, F.; Porcù, E.; Basso, G.; Viola, G. Synthesis, antimitotic and antivascular activity of 1-(3′,4′,5′-trimethoxybenzoyl)-3-arylamino-5-amino-1,2,4-triazoles. *J. Med. Chem.* **2014**, *57* (15), 6795−6808.
(55) Carta, D.; Bortolozzi, R.; Hamel, E.; Basso, G.; Moro, S.; Viola, G.; Ferlin, M. G. Novel 3-substituted 7-phenylpyrrolo[3,2-*f*]quinolin-9(6*H*)-ones as single entities with multitarget antiproliferative activity. *J. Med. Chem.* **2015**, *58* (20), 7991−8010.
(56) Morigi, R.; Locatelli, A.; Leoni, A.; Rambaldi, M.; Bortolozzi, R.; Mattiuzzo, E.; Ronca, R.; Maccarinelli, F.; Hamel, E.; Bai, R.; Brancale, A.; Viola, G. Synthesis, in vitro and in vivo biological evaluation of substituted 3-(5-imidazo[2,1-*b*]thiazolylmethylene)-2-indolinones as new potent anticancer agents. *Eur. J. Med. Chem.* **2019**, *166*, 514−530.
(57) Lin, C. M.; Singh, S. B.; Chu, P. S.; Dempcy, R. O.; Schmidt, J. M.; Pettit, G. R.; Hamel, E. Interactions of tubulin with potent natural and synthetic analogs of the antimitotic agent combretastatin, a structure-activity study. *Mol. Pharmacol.* **1988**, *34*, 200−208.
(58) Clarke, P. R.; Allan, L. A. Cell-cycle control in the face of damage - a matter of life or death. *Trends Cell Biol.* **2009**, *19* (3), 89−98.
(59) Donzelli, M.; Draetta, G. F. Regulating mammalian checkpoints through cdc25 inactivation. *EMBO Rep.* **2003**, *4* (7), 671−677.
(60) Tsujimoto, Y.; Shimizu, S. Role of the mitochondrial membrane permeability transition in cell death. *Apoptosis* **2007**, *12* (5), 835−840.
(61) Xiong, S.; Mu, T.; Wang, G.; Jiang, X. Mitochondria-mediated apoptosis in mammals. *Protein Cell* **2014**, *5* (10), 737−749.
(62) Rovini, A.; Savry, A.; Braguer, D.; Carré, M. Microtubule-targeted agents: when mitochondria become essential to chemotherapy. *Biochim. Biophys. Biochim. Biophys. Acta, Bioenerg.* **2011**, *1807* (6), 679−688.
(63) Romagnoli, R.; Baraldi, P. G.; Salvador, M. K.; Preti, D.; Aghazadeh Tabrizi, M.; Brancale, A.; Fu, X. H.; Li, J.; Zhang, S. Z.; Hamel, E.; Bortolozzi, R.; Porcù, E.; Basso, G.; Viola, G. Discovery and optimization of a series of 2-aryl-4-amino-5-(3′,4′,5′-trimethoxybenzoyl)thiazoles as novel anticancer agents. *J. Med. Chem.* **2012**, *55* (11), 5433−5445.
(64) Romagnoli, R.; Baraldi, P. G.; Salvador, M. K.; Prencipe, F.; Bertolasi, V.; Cancellieri, M.; Brancale, A.; Hamel, E.; Castagliuolo, I.; Consolaro, F.; Porcù, E.; Basso, G.; Viola, G. Synthesis, antimitotic and antivascular activity of 1-(3′,4′,5′-trimethoxybenzoyl)-3-arylamino-5-amino-1,2,4-triazoles. *J. Med. Chem.* **2014**, *57* (15), 6795−6808.
(65) Zamzami, N.; Marchetti, P.; Castedo, M.; Decaudin, D.; Macho, A.; Hirsch, T.; Susin, S. A.; Petit, P. X.; Mignotte, B.; Kroemer, G. Sequential reduction of mitochondrial transmembrane potential and generation of reactive oxygen species in early programmed cell death. *J. Exp. Med.* **1995**, *182* (2), 367−377.
(66) Aredia, F.; Scovassi, A. I. Poly(ADP-Ribose): a signaling molecule in different paradigms of cell death. *Biochem. Pharmacol.* **2014**, *92* (1), 157−163.
(67) Haschka, M. D.; Soratroi, C.; Kirschnek, S.; Häcker, G.; Hilbe, R.; Geley, S.; Villunger, A.; Fava, L. L. The NOXA-MCL1-BIM axis defines lifespan on extended mitotic arrest. *Nat. Commun.* **2015**, *6*, 6891.
(68) Wertz, I. E.; Kusam, S.; Lam, C.; Okamoto, T.; Sandoval, W.; Anderson, D. J.; Helgason, E.; Ernst, J. A.; Eby, M.; Liu, J.; Belmont, L. D.; Kaminker, J. S.; O'Rourke, K. M.; Pujara, K.; Kohli, P. B.; Johnson, Ad. R.; Chiu, M. L.; Lill, J. R.; Jackson, P. K.; Fairbrother, W. J.; Seshagiri, S.; Ludlam, M. J. C.; Leong, K. G.; Dueber, E. C.; Maecker, H.; Huang, D. C. S.; Dixit, V. M. Sensitivity to antitubulin chemotherapeutics is regulated by MCL1 and FBW7. *Nature* **2011**, *471* (7336), 110−114.
(69) Kocab, A. J.; Duckett, C. S. Inhibitor of apoptosis proteins as intracellular signaling intermediates. *FEBS J.* **2016**, *283* (2), 221−231.
(70) Hamel, E.; Lin, C. M. Separation of active tubulin and microtubule-associated proteins by ultracentrifugation and isolation of a component causing the formation of microtubule bundles. *Biochemistry* **1984**, *23* (18), 4173−4184.
(71) Hamel, E. Evaluation of antimitotic agents by quantitative comparisons of their effects on the polymerization of purified tubulin. *Cell Biochem. Biophys.* **2003**, *38* (1), 1−21.
(72) Verdier-Pinard, P.; Lai, J. Y.; Yoo, H. D.; Yu, J.; Marquez, B.; Nagle, D. G.; Nambu, M.; White, J. D.; Falck, J. R.; Gerwick, W. H.; Day, B. W.; Hamel, E. Structure-activity analysis of the interaction of curacin A, the potent colchicine site antimitotic agent, with tubulin and effects of analogs on the growth of MCF-7 breast cancer cells. *Mol. Pharmacol.* **1998**, *53* (1), 62−76.
(73) Salvioli, S.; Ardizzoni, A.; Franceschi, C.; Cossarizza, A. JC-1, but not DiOC6(3) or rhodamine 123, is a reliable fluorescent probe to assess ΔΨ changes in intact cells: implications for studies on

https://dx.doi.org/10.1021/acs.jmedchem.0c01315
J. Med. Chem. 2020, 63, 12023−12042

mitochondrial functionality during apoptosis. *FEBS Lett.* **1997**, *411* (1), 77−82.
(74) *Schrödinger Suite*; Schrödinger LLC: New York, NY, U.S., 2018.
(75) *LigPrep; Maestro; Schrödinger Suites*; Schrödinger, LLC: New York, NY, U.S., 2018.
(76) Shivakumar, D.; Harder, E.; Damm, W.; Friesner, R. A.; Sherman, W. Improving the prediction of absolute solvation free energies using the next generation OPLS force field. *J. Chem. Theory Comput.* **2012**, *8* (8), 2553−2558.
(77) Berman, H. M.; Westbrook, J.; Feng, Z.; Gilliland, G.; Bhat, T. N.; Weissig, H.; Shindyalov, I. N.; Bourne, P. E. The Protein Data Bank. *Nucleic Acids Res.* **2000**, *28* (1), 235−242.
(78) Prota, A. E.; Danel, F.; Bachmann, F.; Bargsten, K.; Buey, R. M.; Pohlmann, J.; Reinelt, S.; Lane, H.; Steinmetz, M. O. The novel microtubule-destabilizing drug BAL27862 binds to the colchicine site of tubulin with distinct effects on microtubule organization. *J. Mol. Biol.* **2014**, *426* (8), 1848−1860.
(79) Gigant, B.; Wang, C.; Ravelli, R. B. G.; Roussi, F.; Steinmetz, M. O.; Curmi, P. A.; Sobel, A.; Knossow, M. Structural basis for the regulation of tubulin by vinblastine. *Nature* **2005**, *435* (7041), 519−522.
(80) Barbier, P.; Dorléans, A.; Devred, F.; Sanz, L.; Allegro, D.; Alfonso, C.; Knossow, M.; Peyrot, V.; Andreu, J. M. Stathmin and interfacial microtubule inhibitors recognize a naturally curved conformation of tubulin dimers. *J. Biol. Chem.* **2010**, *285* (41), 31672−31681.
(81) *Glide*; Schrödinger, LLC: New York, NY, 2018.
(82) Bowers, K. J.; Chow, D. E.; Xu, H.; Dror, R. O.; Eastwood, M. P.; Gregersen, B. A.; Klepeis, J. L.; Kolossvary, I.; Moraes, M. A.; Sacerdoti, F. D.; Salmon, J. K.; Shan, Y.; Shaw, D. E. Scalable algorithms for molecular dynamics simulations on commodity clusters. In *Proceedings of the 2006 ACM/IEEE SC'06 Conference (SC'06)*, Tampa, FL; IEEE, 2006; pp 43−43.
(83) Jorgensen, W. L.; Chandrasekhar, J.; Madura, J. D.; Impey, R. W.; Klein, M. L. Comparison of simple potential functions for simulating liquid water. *J. Chem. Phys.* **1983**, *79* (2), 926−935.
(84) *Prime*; Schrödinger LLC: New York, NY, 2018.

https://dx.doi.org/10.1021/acs.jmedchem.0c01315
J. Med. Chem. 2020, 63, 12023−12042